Paper 41

Employability and Employment Rate of Commerce Students in India: Comparison with Other Streams

Dr. Kritika

Assistant Professor, Department of Commerce, Chaudhary Bansi Lal University, Bhiwani

Ms. Shweta

M.N.S. Government College, Bhiwani

Introduction

Education is the process of skills, moral value or facilitating learning. Education plays an important role in the development of every country. The more educated people in a country, the more developed that country will be. But in India, although the importance of education is increasing and rate of educated people is increasing, people have degrees in their hand but still they are jobless & results in increasing rate of unemployment. So, there are educated people in India but still India is not developing at the rate it should be.That means the problem is in our education system that people are unemployed even after being educated. After 10^{th}, a student has 3 options- science, Commerce and Arts. He has to select one of them.

In this study, the researcher discussed about commerce educated unemployment in India.

Objective of Study

The objective of present study is to analyse the employability and employment rate of commerce students in India.

Commerce

Commerce means activity of buying and selling at large scale. In commerce stream, business related education are provided to the students. In 11^{th}, 12^{th} standard, there are mainly 3 subjects – Business studies, Accountancy and Economics. Commerce is such a vast stream that in graduation & post -graduation level, commerce is divided into so many subjects or fields like –

- Banking

- Human Resource Management
- Corporate Law
- Taxation
- Cost Accountancy
- GST
- Marketing
- International Business & Business Environment
- Business Statistics
- Business Finance
- Auditing
- Organizational Behaviour
- Financial Market Operation
- Import Export Documentation & many more.

There are so many fields in commerce that a commerce student should definitely get a job somewhere but it does not happen. Even after studying commerce at 2 years in school 3 years at graduation level and 2 years at post- graduation level, if a person is still jobless, then there must be some deficiency in our education system.

Rate of Employment in India in 2021 (Degree-wise)

Degree	Rate of Employment
Bachelor of Engineering / Bachelor of Technology	46.82%
M.B.A.	46.59%
B.A.	42.72%
B.Com	40.3%
Bachelor of Pharmaceuticals	37.24%
B.Sc	30.24%
Polytechnic	25.02%
MCA	22.42%

[Ref:- https://www.statistas.com]

According to the data, only 40.3% commerce gradudate are employed & still 59.7% are unemployed in 2021. One of the main reason of increased rate of B.Tech & MBA students is that some practices aspect is included in their curriculum.

Employability among Commerce Graduates across India from 2014 to 2021

Year	Rate of Employability
2021	40.3%
2020	47%
2019	30.06%
2018	33.93%
2017	37.98%
2016	20.58%
2015	26.45%
2014	26.99%

[Ref:- https://www.statista.com]

As per the data, employability rate is highest in 2020 i.e. 47%. But still 53% graduates are unemployed yes, if we look from 2014 to 2021, there has been a huge change in the employment rate, but we can increase it further by making our students ready as per the requirement of Industry.

So, it is the time to make some changes in our education system.

Yes, of course in the past years, there has been a lot of change in our education system like-

- Smart screen replaced chalk Boards
- Online classes during Covid-19 Pandemic
- Free online content availability
- SWAYAM & SWAYAM PRABHA launched in 2017
- MOOC
- National Digital Library and many more.

But the problem is not with 'How they are getting education' whether it is online or offline, but the problem is 'What they are learning'. In Indian education system, more focus is given on Theoretical knowledge rather than practical knowledge at graduation level and that's the reason of increased unemployment.

Example

A commerce graduate person knows what is Auditing, what are its types, it importance, what is included in auditing etc. in theoretical term not in practical term. Practically they don't know how to do auditing.

Commerce graduates find difficulty in getting job as companies hastate to recruit them because they have to spend a lot on their training. Even after studying many fields in commerce, they are not specialized even in any one of them.

In the era of modernization, everything is changing even fields in commerce also.

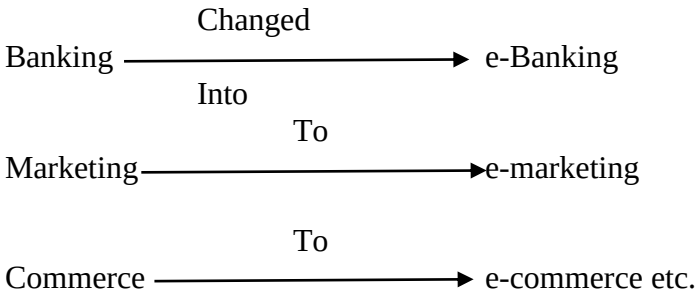

Specialization in every fields is in high demand & specialization comes from practical knowledge. So, it is very important while designing the curriculum of graduation in commerce that it should be made from employer's point of view i.e. what employer wants in an employee while recruiting.

Suggestions

It is high time to change curriculum of graduation.

- Very important to give more emphasis on practical aspects rather than theoretical.
- To change Bachelor of commerce into Bachelor of specific field like Bachelor of Banking, Bachelor of Auditing etc.
- Internship may be included at graduation level.

References

https://www.embibe.com

https://en.m.wikipedia.org

https://www.indiatoday.in

https://www.statista.com

https://www.businesstoday.in

https://www.businessinsider.in

https://timesofindia.indiatimes.com

https://www.indiaapprenticeshipforum.org

HEAT TRANSFER ANALYSIS OF A STRAIGHT FIN WITH TEMPERATURE DEPENDENT PROPERTIES

J. R. WADKAR *, R. G. METKAR **, B. B. PANDIT***

*(Research Scholar, Department of Mathematics, Swami Ramanand Teerth Marathwada University, Nanded, Maharashtra, India.

** (Department of Mathematics, Indira Gandhi Senior College, Nanded, Maharashtra, India.

*** (Department of Mathematics, ShriDatta Arts, Commerce and Science College, Hadgaon, Dist. Nanded, Maharashtra, India.

ABSTRACT:

This problem deals with the determination transient temperature distribution in a thick straight rectangular fin. Initially, the fin is kept at a constant temperature. Convection due to dissipation occurs at all other boundary surfaces. The thermal properties of the material of the fin are assumed to be temperature dependent. The governing nonlinear differential equation is solved by finite difference method. Fundamental theorems of numerical analysis were used to analyze the convergence and stability of a finite difference scheme. The results of temperature has been computed numerically, illustrated graphically and interpreted technically.

KEYWORDS: Straight fin, Transient heat conduction, Non-linear boundary value problem, Finite difference method.

1. INTRODUCTION

Engineers and mathematicians face a difficult task in finding solutions to governing equations that reflect physical systems. Nothing could be more appealing than discovering exact closed form solutions to these equations. However, because nonlinearity occurs in the majority of real-world engineering issues, numerical techniques must be used to acquire the solution.

Cihat Arslanturk [2] used the Adomian decomposition method (ADM) to determine the temperature distribution within straight fins with temperature-dependent thermal conductivity and to evaluate their effectiveness. To examine the annular fin with temperature-dependent thermal conductivity, Huan-Sen Peng et al [3] devised a hybrid numerical technique that incorporates the differential transformation and finite difference method. C. Harley et al.[1] looked at a model that described the temperature profile in a longitudinal fin with a rectangular profile coupled to a fixed base surface. The heat transfer coefficient is expressed as a nonlinear function, whereas thermal conductivity is expressed as a linear function, allowing both to be temperature dependant. Seiyed E. Ghasemi et al. [8] investigated the Differential Transformation Method (DTM), a simple and highly accurate semi-analytical method for solving the nonlinear temperature distribution problem in a longitudinal fin with temperature dependent internal heat generation and thermal conductivity. M.G. Sobamowo [5] used the finite difference approach to investigate heat transmission in a longitudinal rectangular fin with temperature-dependent thermal conductivity and internal heat

generation. K. R. Madhura et al [4] have attempted to investigate the thermal performance of a convective radiative straight porous fin with temperature dependent thermal conductivity and a magnetic field. Various designing and operating parameters such as temperature dependent thermal conductivity parameter, Hartmann number, thermogeometry parameter, radiation parameter, radiation conduction parameter, modified Rayleigh number, and porosity parameter are used to interpret numerical solutions to temperature distribution, efficiency, effectiveness, and heat transfer rate of the porous straight fin.

In this paper an extended straight fin with variable thermal properties is considered. The governing nonlinear differential equation is solved by Finite Difference Method. The results of temperature distribution has been computed numerically, illustrated graphically and interpreted technically.

2. MATHEMATICAL FORMULATION

A thick straight rectangular finis assumed for occupying the space which is defined as $0 \le x \le a,\ 0 \le y \le b,\ 0 \le z \le c$. The three dimensional heat conduction equation of a straight rectangular fin in the transient state is:

$$\frac{\partial}{\partial x}\left(k(T)\frac{\partial T}{\partial x}\right)+\frac{\partial}{\partial y}\left(k(T)\frac{\partial T}{\partial y}\right)+\frac{\partial}{\partial z}\left(k(T)\frac{\partial T}{\partial z}\right)=\rho c_p(T)\frac{\partial T}{\partial t} \qquad (01)$$

The initial condition is

$$T = T_0 \qquad \text{at } t = 0 \qquad (02)$$

The boundary conditions are

$$T = T_b \qquad \text{at } x = 0, t > 0 \qquad (03)$$

$$k(T)\frac{\partial T}{\partial x} = hT \qquad \text{at } x = a, t > 0 \qquad (04)$$

$$k(T)\frac{\partial T}{\partial y} \pm hT = 0 \qquad \text{at } y = 0 \text{ and } y = b,\ t > 0 \qquad (05)$$

$$k(T)\frac{\partial T}{\partial z} \pm h(T) = 0 \qquad \text{at } z = 0 \text{ and } z = c,\ t > 0 \qquad (06)$$

The thermal properties of metals varies with temperature. The thermal conductivity [6] k^{n+1} at the time level n+1 is expresses in term of that at the time level n in the for

$$k^{n+1} \cong k^n + \left(\frac{\partial k}{\partial t}\right)^n \Delta t$$

$$k^{n+1} \cong k^n + \left(\frac{\partial k}{\partial T}\right)^n \left(\frac{\partial T}{\partial t}\right)^n \Delta t$$

Replacing the time derivative and if the thermal conductivity varies linearly with temperature one gets

$$k^{n+1} \cong k^n \left[1 + \beta(T^n - T^{n-1})\right] \tag{07}$$

Similar expression can be written for the specific heat

$$c_p^{n+1} \cong c_p^n \left[1 + \gamma(T^n - T^{n-1})\right] \tag{08}$$

where, β is temperature coefficient of thermal conductivity,

γ is temperature coefficient of specific heat.

Equations (1) to (8) constitute the mathematical formulation of the problem.

3. MATHEMATICAL SOLUTION

The Crank Nicolson finite difference method is applied [6] to solve the nonlinear boundary value problem defined by (1) to (6). One can divide the *x, y, t* domain into small intervals $\Delta x,\ \Delta y, \Delta z,\ \Delta t$ such that

$x = i\Delta x \quad i = 0,1,.....N \ \ (N\Delta x = a)$

$y = j\Delta y \ \ j = 0,1,2,.....M\,(M\Delta y = b)$

$z = k\Delta z \ \ k = 0,1,2,.....P(P\Delta z = c)$

$t = n\Delta t \quad n = 0,1,2,.....$

The dependent variable at the nodal point $(i\Delta x,\ j\Delta y, k\Delta z)$ at the time $n.\Delta t$ is denoted by

$$T(i.\Delta x,\ j.\Delta y, k.\Delta z) = T_{i,j,k}^{n}$$

The Crank Nicolson finite difference representation [8] of the two dimensional nonlinear heat equation (1) is given by

$$\rho(c_p)_{i,j,k}\frac{T_{i,j,k}^{n+1}-T_{i,j,k}^{n}}{\Delta t}=\frac{1}{2}\left[k_{i-1/2,j,k}\frac{T_{i-1,j,k}^{n+1}-T_{i,j,k}^{n+1}}{(\Delta x)^2}+k_{i+1/2,j,k}\frac{T_{i+1,j,k}^{n+1}-T_{i,j,k}^{n+1}}{(\Delta x)^2}\right]$$
$$+\frac{1}{2}\left[k_{i-1/2,j,k}\frac{T_{i-1,j,k}^{n}-T_{i,j,k}^{n}}{(\Delta x)^2}+k_{i+1/2,j,k}\frac{T_{i+1,j,k}^{n}-T_{i,j,k}^{n}}{(\Delta x)^2}\right]$$
$$+\frac{1}{2}\left[k_{i,j-1/2,k}\frac{T_{i,j-1,k}^{n+1}-T_{i,j,k}^{n+1}}{(\Delta y)^2}+k_{i,j+1/2,k}\frac{T_{i,j+1,k}^{n+1}-T_{i,j,k}^{n+1}}{(\Delta y)^2}\right]$$
$$+\frac{1}{2}\left[k_{i,j-1/2,k}\frac{T_{i,j-1,k}^{n}-T_{i,j,k}^{n}}{(\Delta y)^2}+k_{i,j+1/2,k}\frac{T_{i,j+1,k}^{n}-T_{i,j,k}^{n}}{(\Delta y)^2}\right]$$
$$+\frac{1}{2}\left[k_{i,j,k-1/2}\frac{T_{i,j,k-1}^{n+1}-T_{i,j,k}^{n+1}}{(\Delta z)^2}+k_{i,j,k+1/2}\frac{T_{i,j,k+1}^{n+1}-T_{i,j,k}^{n+1}}{(\Delta z)^2}\right]$$
$$+\frac{1}{2}\left[k_{i,j,k-1/2}\frac{T_{i,j,k-1}^{n}-T_{i,j,k}^{n}}{(\Delta z)^2}+k_{i,j,k+1/2}\frac{T_{i,j,k+1}^{n}-T_{i,j,k}^{n}}{(\Delta z)^2}\right] \quad (09)$$

The subscript $i\pm 1/2$ for the thermal conductivity denotes that a mean value of thermal conductivity between the nodal points $i\pm 1$ and i.

Solving (9) for $T_{i,j}^{n+1}$ and setting square grids $\Delta x=\Delta y=\Delta z$ one gets the recursive relation,

$$T_{i,j,k}^{n+1}=A_{ijk}T_{i-1,j,k}^{n+1}+B_{ijk}T_{i+1,j,k}^{n+1}+C_{ijk}T_{i,j-1,k}^{n+1}+D_{ijk}T_{i,j+1,k}^{n+1}+E_{ijk}T_{i,j,k-1}^{n+1}+F_{ijk}T_{i,j,k+1}^{n+1}-G_{ijk}T_{i,j,k}^{n+1}+b_{ijk} \quad (10)$$

where

$$A_{ijk}=\frac{k_{i-1/2,j,k}\Delta t}{2(\Delta x)^2\rho(c_p)_{i,j,k}}$$

$$B_{ijk}=\frac{k_{i+1/2,j,k}\Delta t}{2(\Delta x)^2\rho(c_p)_{i,j,k}}$$

$$C_{ijk}=\frac{k_{i,j-1/2,k}\Delta t}{2(\Delta y)^2\rho(c_p)_{i,j,k}}$$

$$D_{ijk} = \frac{k_{i,j+1/2,k}\Delta t}{2(\Delta y)^2 \rho(c_p)_{i,j,k}}$$

$$E_{ijk} = \frac{k_{i,j,k-1/2}\Delta t}{2(\Delta y)^2 \rho(c_p)_{i,j,k}}$$

$$F_{ijk} = \frac{k_{i,j,k+1/2}\Delta t}{2(\Delta y)^2 \rho(c_p)_{i,j,k}}$$

$$G_{ijk} = A_{ijk} + B_{ijk} + C_{ijk} + D_{ijk} + E_{ijk} + F_{ijk}$$

$$b_{ijk} = A_{ijk}T^n_{i-1,j,k} + B_{ijk}T^n_{i+1,j,k} + C_{ijk}T^n_{i,j-1,k} + D_{ijk}T^n_{i,j+1,k} + E_{ijk}T^n_{i,j,k-1} + F_{ijk}T^n_{i,j,k+1} + (1 - G_{ijk})T^n_{i,j,k} \quad (11)$$

and truncation error is of order $O\left[(\Delta t)^2, (\Delta x)^2, (\Delta y)^2, (\Delta z)^2\right]$ and the scheme is unconditionally stable.

The finite difference approximation for initial and boundary conditions,

Initially at $t = 0$

$$T^0_{i,j,k} = T_0 \quad (12)$$

At initial edge ($x = 0$)

$$T^n_{1,j,k} = T_b \quad (13)$$

At parallel extreme edge ($x = a$)

$$T^n_{i+1,j,k} = T^n_{i-1,j,k} + \frac{2h\Delta x}{k(T)} T^n_{i,j,k} \quad (14)$$

At initial edge and extreme edge ($y = 0$ and $y = b$)

$$T^n_{i,j+1,k} = T^n_{i,j-1,k} + \frac{2\Delta y}{k(T)} T^n_{i,j,k} \quad (15)$$

The initial edge and extreme edge ($z = 0$ and $z = c$)

$$T^n_{i,j,k+1} = T^n_{i,j,k-1} + \frac{2\Delta z}{k(T)} T^n_{i,j,k} \quad (16)$$

Equation (12) gives the initial value of temperature T at each grid point of the plate (at $t = 0$).

Assuming that the coefficients A_{ijk}, B_{ijk}, C_{ijk}, D_{ijk}, E_{ijk}, F_{ijk}, b_{ijk} are known for each iteration equation (10) with the boundary conditions (13) to (16) gives a set of linear equations, one can apply the successive over relaxation method to solve these equations. The recursive relation is given by,

$$T_{i,j,k}^{n+1} = (1-\omega)T_{i,j,k}^{n} + \omega\,[A_{ijk}T_{i-1,j,k}^{n} + B_{ijk}T_{i+1,j,k}^{n} + \mathrm{C}_{ijk}T_{i,j-1,k}^{n} + D_{ijk}T_{i,j+1,k}^{n} + \mathrm{E}_{ijk}T_{i,j,k-1}^{n} + F_{ijk}T_{i,j,k+1}^{n} - G_{ijk}T_{i,j,k}^{n} + b_{ijk}\,] \quad (17)$$

Where relaxation factor ω lies between 1 and 2

The truncation error is of order $O\left[(\Delta t)^2,(\Delta x)^2,(\Delta y)^2,(\Delta z)^2\right]$, the scheme is unconditionally stable and convergent by using following theorem due to Lax [10].

Theorem1: A consistent difference scheme for a well posed linear initial boundary value problem is convergent if and only if it is stable.

4. NUMERICAL CALCULATIONS

The fin is divided in equal grids of $\Delta x = \Delta y = \Delta z$ =0.02 meters. Number of iterations has been performed for each time step of Δt =0.1seconds.

The simultaneous equations formed by using (13) to (16) in equation (17) are solved by using MATLAB programming.

A. Dimensions

Length of rectangular fin $a = 1\ m$,

Breadth of rectangular fin $b = 0.1\ m$,

Thickness of rectangular fin $t_c = 0.01\ m$.

B. Material properties

The numerical calculation has been carried out for anAluminiumfin with the material properties as,

Thermal conductivity $k_0 = 204.2\ W/mK$,

Specific heat $c_p = 896\ \mathrm{J}/KgK$,

Thermal diffusivity $\alpha = 84.18\mathrm{x}10^{-6} m^2/\mathrm{s}$,

Density $\rho = 2707 Kg/m^3$,

Coefficient of convection $h = 10$,

Coefficient of convection at ($x = 0$) surface $h_1 = 100$,

Initial Temperature of the fin $T_0 = 300K$,

Initial Temperature of the fin $T_b = 400K$,

Temperature at grid points equally spaced with $\Delta x = \Delta y = \Delta z$ =0.02 meters and at time t = 200x0.1 = 20 seconds is calculated. The surface plots for temperature for variable thermal properties are given below:

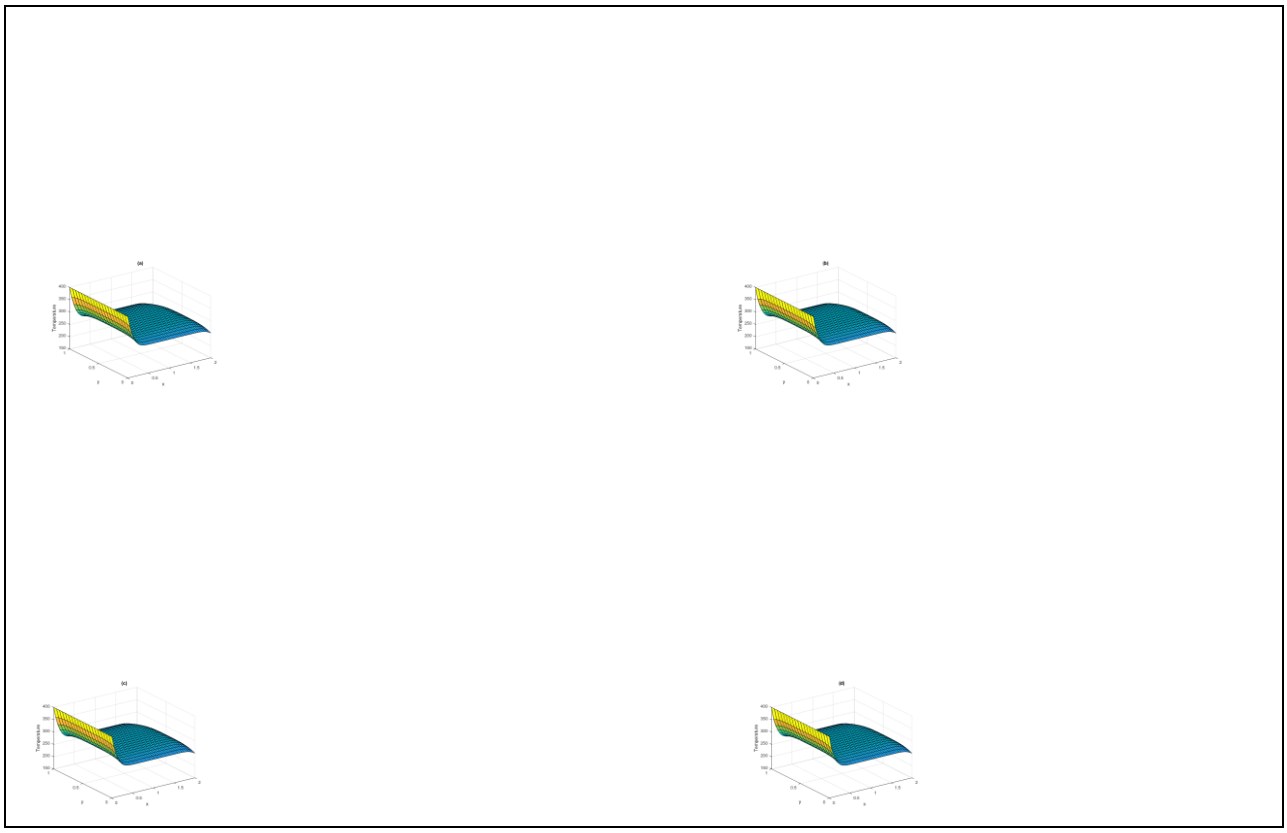

Fig.1: Temperature distribution for (a) $\beta = 0, \gamma = 0$, (b) $\beta = 0.001, \gamma = 0$, (c) $\beta = 0, \gamma = 0.001$, (d) $\beta = 0.001, \gamma = 0.001$

The figures show that when the thermal properties are dependent and independent of temperature, there is a difference in temperature distribution. All of the extreme edges experience convection due to dissipation.

5. CONCLUDING REMARKS

The goal of this paper is to explain the relevance of temperature-dependent thermal characteristics in heat transfer studies. The mathematical formulation of a physical application in the form of a boundary value problem is highly non-linear due to the consideration of temperature dependent thermal properties. The finite difference technique for governing non-linear partial differential equations has been established to find mathematical solutions to non-linear boundary value problems. Fundamental theorems of Numerical Analysis were used to analyze the convergence and stability of finite difference solutions. When the thermal properties are independent

($\beta = 0, \gamma = 0$) and dependent ($\beta \neq 0, \gamma \neq 0$) on temperature, the comparison is performed for the temperature at each nodal point.

To summarize, temperature dependent thermal properties play an essential role in heat transfer studies, especially when a solid is exposed to considerable temperature variations. This study provides a more detailed outline for solving non-linear boundary value problems. This method can be used to deduce any special case of interest.

REFERENCES

[1] C. Harley and R.J. Moitsheki, "Numerical investigation of the temperature profile in a rectangular longitudinal fin", *Nonlinear Analysis: Real World Applications*, Vol. 13 ,pp 2343–2351,2012.

[2] Cihat Arslanturk, "A decomposition method for fin efficiency of convective straight fins with temperature-dependent thermal conductivity", *International Communications in Heat and Mass Transfer, Vol*. 32 pp. 831–841, 2005.

[3] Huan-Sen Peng and Chieh-Li Chen , "Hybrid differential transformation and finite difference method to annular fin with temperature-dependent thermal conductivity", *International Journal of Heat and Mass Transfer, Vol*. 54, pp. 2427–2433, 2011.

[4] K. R. Madhura, Babitha, G. Kalpana1 and O. D. Makinde, "Thermal performance of straight porous fin with variable thermal conductivity under magnetic field and radiation effects", *Heat Transfer* pp.1–18, 2020.

[5] M.G. Sobamowo, "Analysis of convective longitudinal fin with temperature-dependent thermal conductivity and internal heat generation", *Alexandria Engineering Journal*, Vol. 56, pp. 1-11, 2017.

[6] M.Necati Ozisik, *Heat conduction*, John Wiley and Sons, Inc.1993.

[7] Ozisik M.N., *Boundary value problem of heat conduction*, International Text book Company, Scranton, Pennsylvania, 1968.

[8] Seiyed E. Ghasemi ,M. Hatami and D. D. Ganji , "Thermal analysis of convective fin with temperature-dependent thermal conductivity and heat generation", *Case Studies in Thermal Engineering* ,vol.4,pp1–8,2014.

[9] Thomas J.W., *Numerical Partial Differential Equation: Finite Difference Methods, Springer-Verlag*, New York, 1995.

[10] Thomas J.W. ,*Numerical Partial Differential Equation: Conservation Laws and Elliptic Equations, Springer-Verlag*, New York, 1995.

Paper 43

Ethan botanical study of Nagzira Wildlife Sanctuary, Gondia district, Maharashtra, India.

Patil D. N.

Department of Botany, BJS's A.S.C. College, Pune-Nagar Road, Wagholi, Pune.

Abstract- Ethnic people found in the areas are 'Gond'. Plants used by them for their day-to-day life for food, shelter, clothing and medicines are mentioned in detail under economic and medicinal plants, including wild relatives of cultivated plants also. The area is very rich with economic and medicinal plant wealth. Economically, plants used for food, fodder, shelter for wild animals & birds, timber, fiber, minor forest products and for medicines are mentioned. Glimpses of this wealth in the form of museum are established near 'Pitezari'area of Nagzira Wildlife Sanctuary. The account of this wealth (c 300 spp.) is depicted as under as well as notes of individual plants in systematic enumeration.

Keywords : Ethnic people, Wildlife, Wild relative

Introduction-

Plants have many and diverse uses which have direct or indirect bearing on the civilization of human society. India is a vast country with it's main land area about 3,287 million sq. km and a coastline of over 7,500 km and is the second largest country in Asia and seventh in the world. Over and above, with diversity of climate, soil and topography with almost all types of ecosystems found anywhere in the world and hundreds of biotopes -each supporting rich characteristic floristic and Faunistic elements with Eurasian , Afro tropical and Indo-Malayan floristic elements, India harbors over 45,000 species of plants (c 11 percent of world's flora). This includes Bacteria and viruses (850 spp.), Algae (6,500 spp.), Fungi (14,500 spp.), Lichens (2,021 spp.), Bryophytes (2,850 spp.) , Pteridophytes (1,200 spp.), Gymnosperms (48 spp.) and Angiosperms (17,500 spp.). Among them are number of plants with botanical interest e.g. insectivorous (c 41 spp.), Orchids (c

1087 spp.) and Parasites (c135 spp.).Because of this rich diversity, India is recognized as one of the 12 mega diversity regions of the world (Kothari & Singh,1998; Singh & Singh,2002).

About the Study Area-

. Nagzira Wildlife Sanctuarty,Maharashtra, India. (Map-4)

The wildlife Sanctuary (Bio geographical Province 6D) was constituted as per the notification No. WLP/1669/22860/Y/dt.3/6/1970, covering an area *152.81 sq. km*. The Sanctuary is miraculously preserved as 'Green Oasis' in the eastern most part of the Maharashtra State and has a great importance from bio-diversity conservation point of view. The name Nagzira Wildlife Sanctuary is based on idol Nagdev and Nagzira lake.

Location: The Sanctuary is situated in Sakoli tahsil of Bhandara district and Arjuni (Sadak), Goregaon & Tiroda tahsil of Gondia District (Maharashtra State) under the Nagzira range at 79^{o} 58' E to 80 ^{o} 11'E longitude and 21 ^{o}12' N to 21 ^{o} 21' N latitude.

Bio-geographic Zonation: As per the wildlife Institute of India, Dehradun, This Sanctuary is classified as follows: 1)Bio-geographical Kingdom- Paleotopical. 2)Sub-Kingdom-Indomalyosian. 3) Bio-geographical Zone-6- Deccan peninsula. 4)Biotic Province -6B-Central Deccan. The Bio-geographic zone is one of the least protected zone in India though rich in floral and faunal diversities. Hence it needs tall degree of protection. The entire area [152.81 sq. km,old Reserved Forest] of this Sanctuary is covered by 4 Topo-sheets bearing numbers 55(0/15), 55(0/16), 64(C/3) & 64(C/4).

Boundaries: The total length of external boundary is 104.53 km out of which 74.93 km is an artificial boundary and 29.60 km is natural boundary as under.

On the north: Revenue village boundary of the village Kursipar, Berdipar, Belapur, Hamesha, Kodebarra, Mangezari.*On the East*: Railway line Gondia to Chandrapur, broad guauge section of S.E. Railway.*On the South*: Pitezari fazal forests and Sakoli range, village boundaries of Jamdi, Kosamtondi and Reserved forest boundary.*On the West*: Village boundary of Bhajepar, Chorkhamara, Chorkhamara-Pangdi cart track and Reserve forest boundary.

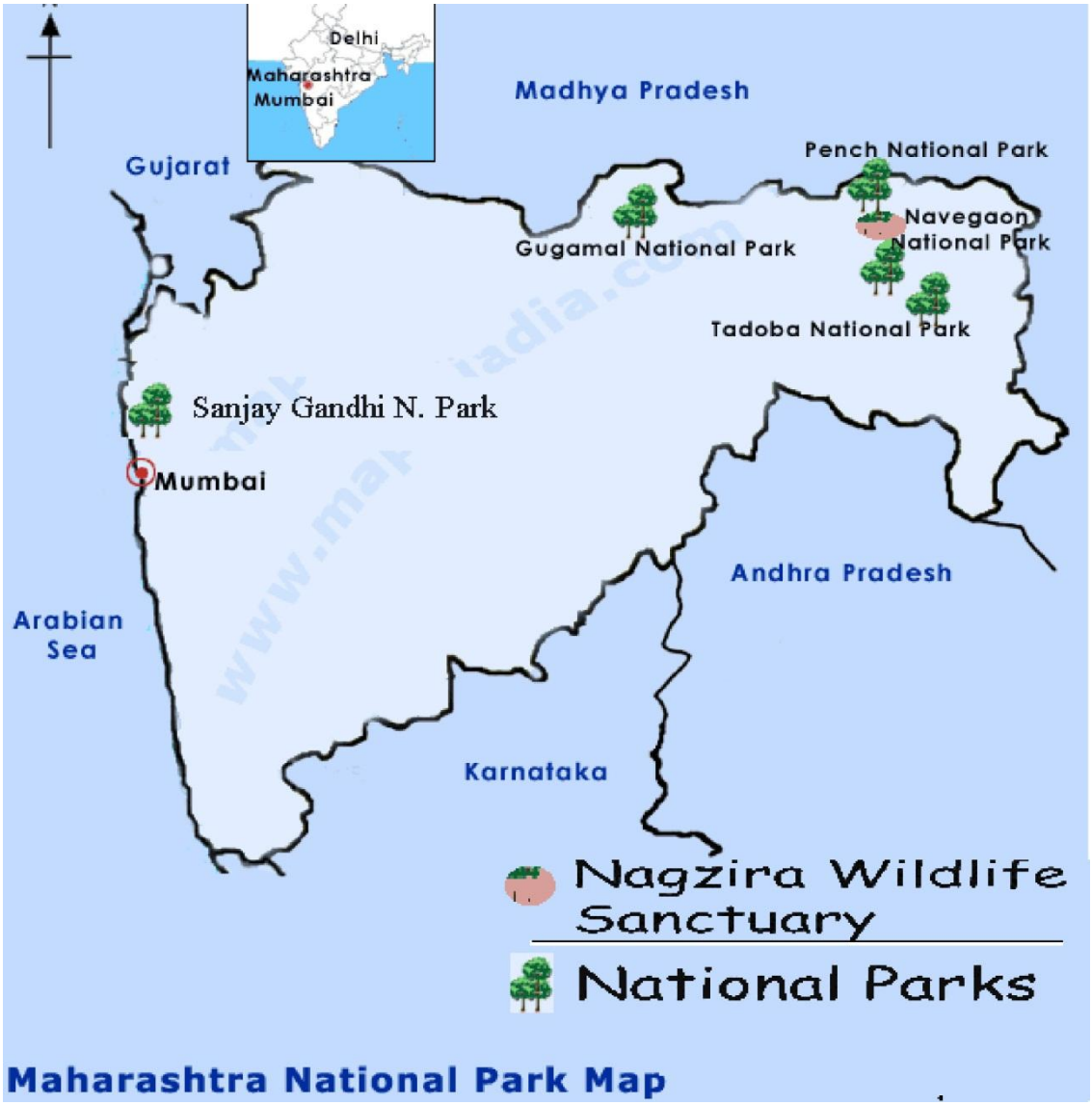

The Sanctuary is surrounded externally by the Reserve forests of Gondia forest division and Bhandara Forests Division on the Northern and Eastern side and by Reserve Forests of FDCM of Bhandara Division on the Southern and Western side. The length of internal range of boundary is 104.53 km. 'Thadezari' is the only village geographically situated inside the Sanctuary, coincide the Compartment boundry

Methodology-

To study the floristic composition of the Nawegaon National Park and Nagzira Wildlife Sanctuary , plant exploration tours were arranged in different seasons during. Flowering and fruiting specimens were collected. Field observations regarding habit, habitat, colour of the flowers, local names, relative abundance, associated plants etc. were noted .Close-up of flowering

/ fruiting material and habit along with associated plants were also photographed. Plants were processed in customary way and studied in the regional herbarium of Botanical Survey of India, Pune and deposited *(BSI)*.

Result and Discussion-

The present study mainly deals with flowering plants of Nawegaon National Park and Nagzira Wildlife Sanctuary . It includes 715 species belonging to 440 genera spread over 122 families of Angiosperms. Besides the Angiosperms, 7 Pteridiophytes were also recorded from the study areas.

General Survey –Table-I

GROUPS	Families	Genera	Species
Monocot	022	090	145
Dicot	100	350	570
Pteridophytes	07	07	07
Total	**129**	**447**	**722**

Medicinal plants: There are c 300 number of plants used for medicines, few of them are (c34) are mentioned in Table-II

Table -II

S. No.	**Name of the plant & family**	**Local names**	**Parts used for cure**
1.	*Abrus precatorius* L. FABACEAE	Gunja	**Roots**-Cold, cough, sore throat.
2.	*Abutilon indicum* (L.) Sweet MALVACEAE	Petari	**Leaves**-Diabetes. **Seeds**-Cough, piles, laxative.
3.	*Acacia catechu* (L.f.) Willd. MIMOSACEAE	Khair	**Bark**-Asthma, Bronchitis, blood purifier, skin diseases.
4.	*Achyranthes aspera* L. AMARANTHACEAE	Aghada	**Roots,Seeds**–Bronchitis, rheumatic , tooth ache. **Whole plant**- Cough,, piles.
5.	*Argemone mexicana* L. PAPAVERACEAE	Pivla-dhotra	**Roots,Leaves,Seeds**-Scabies. **Whole plant**- Jaundice.
6.	*Aristolochia indica* L. ARISTOLOCHIACEAE	Sapasan	**Roots**-Diarrhoea. **Whole plant**-Snake-bite.
7.	*Bombax ceiba* L. BOMBACACEAE	Sawar	**Fruits**-Pain killer. Water extract of thorns for pimples.

8.	*Bridelia retusa* (L.) Spreng. EUPHORBIACEAE	Asana	**Leaves, Fruits**-Diabetes.
9.	*Boswelliaserrata*Roxb.ex Coleb. BURSERACEAE	Salai	**Bark**-Antiseptic,cold, stomach pain.
10.	*Buchanania cochinchinensis* (Lour.) Almeida ANACARDIACEAE	Charoli	**Seeds**-Digestive, brain tonic. **Seed oil**-Protection against white ants.
11.	*Butea monosperma* (Lam.) Taub. FABACEAE	Palas	**Root bark**-Blood Pressure. **Leaves**-Eye diseases. **Flowers**-Cough, leprosy. **Seeds**-Dysentery, ring worm.
12.	*Caesalpinia bonduc* (L.) Roxb. CAESALPINIACEAE	Sagargota	**Seed oil**-Rheumatic pains, skin diseases.
13.	*Capparis sepiaria* L. CAPPARACEAE	Kanthatara, Pachra	**Bark, roots**-Dropsy, Gout.
14.	*Careya arborea* Roxb. LECYTHIDACEAE	Kumbhi	**Bark**-Fistula, Stomach pain, snakebite **Flowers**-Tonic after delivery to women. **Calyx**-Cold, cough..
15.	*Celastrus paniculatus* Willd. CELASTRACEAE	Malkangoni	**Bark**-Wounds.
16.	*Cleistanthus collinus* (Roxb.) Benth. ex Hook.f. EUPHORBIACEAE	Garari	**Bark**- Wound healing and skin disease.
17.	*Cordia dichotoma* Forst. f. BORAGINACEAE	Bhokar	**Bark**-Cough, sore throat. **Fruits**-Cough, Chest pain, Urinary disorder.
18.	*Elephantopus scaber* L. ASTERACEAE	Rantambaku	**Roots**-Tooth-ache, Vomiting, ulcer. **Roots, Leaves**-Snake bite, Eczema, Dysentery.
19.	*Gardenia gummifera* L.f RUBIACEAE	Dikemali, Kamarri	**Gum**-Antiseptic, constipation.
20.	*Gloriosa superba* L**.** LILIACEAE	Khadyanag	**Roots**-Leprosy, scabies, piles, snake bite.
21.	*Helicteres isora* L. STERCULIACEAE	Murud-sheng	**Roots**-Diabetes. **Bark, fruits**-Dysentery.
22.	*Hemidesmus indicus* (L.) Schult. PERIPLOCACEAE	Anantvel	**Roots**-Stomach cure, skin disease.
23.	*Holarrhena pubecens* (Buch.-Ham.) Wall. ex G. Don APOCYNACEAE	Pandhra-kuda	**Roots**-Spleen, Urinary cure. **Bark**-Bronchitis. **Flower, seeds**-Skin disease.
24.	*Jatropha gossypifolia* L.	Mogli-Erand	**Stem**-Tooth ache.

	EUPHORBIACEAE		
25.	*Lannea coromandelica* (Houtt.) Merr. ANACARDIACEAE	Moya, Shimti	**Bark**-cough, wounds. **Leaves**-swelling, Elephantiasis. **Gum**-edible.
26.	*Mallotus philippensis* (Lam.) Muell.-Arg. EUPHORBIACEAE	Kumkum	**Bark**-Leprosy. **Fruits**-Abortion, purgative.
27.	*Plumbago zeylanica* L. PLUMBAGINACEAE	Chitrak	**Roots**-Spleen, skin disease, piles, liver cure. **Root-bark**-antiperiodic.
28.	*Pongamia pinnata* (L.) Pierre FABACEAE	Karanj	**Leaves**-Diarrhoea, fever **Bark**-piles, stomach pain **Seeds,Seed-oil**-Skin diseases.
29.	*Pterocarpus marsupium* Roxb. FABACEAE	Chikna, pale-asan	**Gum**-Asthama in children **Stem, bark**-Bone fracture, tonic. **Leaves**-skin disease. **Flowers**-Urinary disorder.
30.	*Rauvolfia serpentina* (L.) Benth. ex Kurz APOCYNACEAE	Sarpgandha	**Roots**-Blood pressure. **Leaf juice**-vomiting. **Whole plant**-snake bite.
31.	*Solanum virginianum* L. SOLANACEAE	Kate-ringni Ran-wangi	**Berries vapour**-Tooth ache.
32.	*Soymida febrifuga* (Roxb.) A. Juss. MELIACEAE	Rohan	**Bark**-Diarrhoea, dysentery.
33	*Terminalia bellirica* Roxb. COMBRETACEAE	Beheda	**Fruits,Seeds**-Asthma, Bronchitis, stomach disorder, piles, leprosy.
34.	*Woodfordia fruticasa* (L.) Kurz LYTHRACEAE	Dhayti	**Flowers paste**-Injuries, dysentery, cough, small pox. **Fruits**-Tonic.

References-

CHAMPION, H.G.& S.K.SETH, 1968. *A revised Survey of Forest Types of India,* Managers of Pub., Delhi.

CHATTERJEE, D. 1962. Florestic patterns of Indian vegetation in *Proc. Summer School in Bot.* New Delhi, Darjeeling pp. 32-42. Calcutta.

DHARANKAR, C. M. 1976. *Checklist of Birds, Nawegaon National Park.*

DIXIT, R. D. 1984. *A census of the Indian Pteridophytes, Botanical Survey of India,* Dept. of Environment, New Delhi.

ILLORKAR,V.M.& N.G.Totey 1999. *Regeneration Status of Nawegaon National Park* (Maharashtra) Indian J. Fores.Vol. 22 (3) : 203-209.

ILLORKAR,V.M. & P.K.KHATRI 2003. *Phytosociological Study of Nawegaon National Park* (Maharashtra) p. 377. IUCN, 1972. *World Heritage* Convention concerning the Protection of World Cultural and Natural Heritage.

S. KARTHIKEYAN, M. SANJAPPA & S. MOORTHY 2009. *Flowering Plants of India, Dicotyledons vol. 1*.(Acanthaceae- Avicenniaceae) Botanical Survey of India, Kolkata.

KOTHARI, M. J., & K.M. RAO, 1999. Ethanobotanical Studies in Thane district, Maharashtra . *J. Econ. Tax. Bot.* 23(2): 265 -272.

KOTHARI, M. J., & N. P. SINGH, 1998. Mangrove diversity along the North-West coaof India. *J. Econ. Tax. Bot*. 22 (3): 571-585.

KOTHARI, M. J., & N.P.SINGH, 2002. Fragile ecosystems, Kutch in Singh, N. P. & K. P. Singh (eds.) *Floristic Diversity and conservation Strategies in India* 2877- 2898. Botanical Survey of India,Kolkata.

MALHOTRA , S. K. & K.M. RAO, 1982. A Vegetation Of Nawegaon National Park and its Environ. Maharashtra State, *Bull. Bot.Surv.India* Vol.22,(1-4): 1-11 .

MALHOTRA , S. K. & K.M. RAO, 1981a. A contribution to the Flora of Bhandara District, Maharashtra State (India), *J. Econ . Tax . Bot* . 2 : 107-136.

MALHOTRA , S. K. & K.M. RAO, 1981b. The Vegetation of Nagzira Wildlife Sanctuary and its Environs. Maharashtra State. *J. Bombay Nat. Hist. Soc.* 78(3): 475-486.

PATIL, D. N. , & M.J. Kothari , 2013 a. *Floristic Diversity of Nagzira Wildlife Sanctuary in Gondia Dist., Maharashtra State, published in Biodiversity and Environment J. Science Information , spl. Vol. 7; 83-88.*

Paper 44

Study of dielectric and electrical properties of aqueous L-phenylalanine in the frequency range of 20 Hz to 2 MHz

D G Rathod[1] , D N Rander[1] , K S Kanse[1], Y S Joshi[1*], A C Kumbharkhane[2]

Deptt. of Physics and Electronics, Lal Bahadur Shastri Mahavidyalaya, Dharmabad, Dist. Nanded (MS) India

School of Physical Sciences, Swami Ramanand Teerth Marathwada University, Nanded (MS) India

Abstract:

Precision LCR meter technique has been extensively used to study complex relative dielectric and electric properties of amino acids. Using precision LCR meter technique, complex relative dielectric permittivity spectra of L-phenylalanine were obtained in the frequency range of 20Hz to 2 MHz for various concentrations at 25^0C. The Complex dielectric function $\varepsilon^*(\omega)$, static dielectric constant (ε_0), dielectric loss (tan δ), electric modulus $M^*(\omega)$, electrical conductivity $\sigma^*(\omega)$have been studied and electrode potential relaxation time (τ_{EP}) from dielectric loss peak and ionic conductivity relaxation time (τ_σ) have been extracted from the imaginary part of electric modulus M".

Keywords:

Precision LCR meter, Static dielectric permittivity, Electric modulus, L-phenylalanine.

Introduction:

L-phenylalanine is an essential aromatic amino acid in humans provided by food having molecular formula $C_9H_{11}NO_2$ andit has phenyl and indole ringsshown in Fig.1and exhibits non linear optical property[1]. Major dietary sources of L-phenylalanine include meat, fish, eggs, cheese, and milk. L-phenylalanine is most commonly used for a skin disorder that causes white patches to develop on the skin. Phenylalanine plays a key role in the biosynthesis of other amino acids and is important in the structure and function of many proteins and enzymes e.g. it is converted to tyrosine used in the biosynthesis of dopamine and noradrenaline neurotransmitters.

L-phenylalanine is essential protein exhibits the properties such as Non linear optical (NLO), thermal stability, negative photoconductivity and low dielectric loss make the material suitable for NLO device fabrication[1-8]. These crystals were grown by slow evaporation [1,6-9] and studied using TGAtechnique [7] and vibrational and structural properties using FTIR [10].Electrical and dielectric properties properties such as electric conductivity, complex dielectric function, Electric modulus were studied using precision LCR meter [11-14]. Dielectric study of phenylalanine was studied by using TDR [15]. However, literature survey elucidates high scarcity in the dielectric properties using precision LCR meter.Dielectric response provides information such as structural characteristics of biomolecules, membrane and interfacial properties of molecular film, water content and its effect as plasticizer and lyophilization of proteins [16-18].

Water is a polar and hydrogen bonded liquid. It is the basic of all living organism therefore it important to study the dielectric properties of aqueous L-phenylalanine. In present

study, the complex permittivity spectra of L-phenylalanine and water mixtures at 25°C between mole fraction range Xw=1.0 to Xw=0.9972 have been measured using precision LCR meter in the frequency range of 20Hz to 2MHz. The electrical and dielectric properties of the aqueous solution are represented in terms of complex dielectric function ε*(ω), electrical modulus M*(ω), electrical conductivity σ*(ω). This data might be useful to characterize and analyze pharmaceutical material, food processing industry and in solubility prediction method in aqueous solution[15-16].

2. Experimental

2.1. Materials

The L-phenylalanine and water were commercially obtained from Fisher Scientific with 99% purity and were used without further purification. The L-phenylalanine-water solutions were prepared at different gravimetric percentage.

2.2 Measurement

The complex relative dielectric function ε*(ω) of aqueous solution of L-phenylalanine were determined by using Agilent E4980A precision LCR meter. A four terminal dielectric test fixture, Agilent 16452A was used for capacitance and resistance measurement in the frequency range 20Hz to 2MHz. The capacitance and parallel resistance of the liquid dielectric test fixture without and with samples were measured to compensate for a short [19]. The test fixture correction coefficient was also considered to cancel the effect of stray capacitance during the evaluation of the value of the complex dielectric function. The complex dielectric function ε*(ω) of the materials is determined using Eq.1

$$\varepsilon^*(\omega) = \varepsilon'(\omega) - j\varepsilon''(\omega) = \alpha\left[\frac{C_p}{C_o} - j\frac{1}{\omega C_o R_P}\right] \qquad (1)$$

Where ω=2πf is the angular frequency and α is the correction coefficient of the cell.

3. Results and Discussion

3.1 Complex relative permittivity

Fig. 2 shows the frequency dependent dielectric spectra of the real part of the relative dielectric function ε' for aqueous L-phenylalanine solution. It is observed that the dielectric permittivity for pure water and solution have very high value at lower frequency and these values lowers with increase in frequency. The dielectric permittivity values for aqueous L-phenylalanine have high value in lower frequency region and decreases rapidly with the increase in the frequency up to 50KHz. Above this frequency range dielectric permittivity becomes almost independent of the frequency. The large value of dielectric permittivity of aqueous solution in the low frequency range is due to the electrode polarization effect. The EP phenomena occurs due to formation of electric double layer (EDL) capacitances by the free charges build up at the interface between the electrolyte and electrode surfaces.

Frequency dependent spectra of dielectric loss, tan δ for L-phenylalanine water mixtures shown in Fig.3. The tan δ spectra has the loss peak value corresponding to the electrode polarization relaxation frequency f_{EP}, which is used to evaluate the electrode polarization relaxation time, $\tau_{EP} = (2\pi f_{EP})^{-1}$[20,21].

The electrode polarization relaxation times (τ_{EP}) for aqueous solution are plotted in Fig. 4. The τ_{EP}involves charging and discharging time of EDL capacitance, which is associated with the overall dynamics of the absorbed ions on the electrode surfaces in the alternating electric field.τ_{EP} found to be 50.20 μs for water is highest in overall concentrationat electrode polarization relaxation frequency 3169 Hz.τ_{EP} value decreases constantly up to mole fraction 0.999 of water with the addition of L-phenylalanine in water and lowest (5.63 μs) at 28250 Hz at Xw = 0.9989, thereafter it fluctuates but does not show rapid changes.

3.2 Electrical modulus:

The frequency dependent values of M*(ω) [22,23]is obtained using

$$M^*(\omega) = \frac{1}{\varepsilon^*(\omega)} = M' + jM'' = \frac{\varepsilon'}{\varepsilon'^2 + \varepsilon''^2} + j\frac{\varepsilon''}{\varepsilon'^2 + \varepsilon''^2} \quad (2)$$

The complex electric modulus M' and M'' for L-phenylalanine–Water mixture are shown in Fig.5 shows M'' peak value, the frequency f_σ corresponding to these peaks is related to the most probable ionic conductivity relaxation time $\tau_\sigma = (2\pi f_\sigma)^{-1}$[21].From the graph of M''(ω), ionic conductivity relaxation time (τ_σ) corresponding to the peak values of M''(ω) are determined. These values are systemized in Table 1. Addition of water in L-phenylalanine cause the peak of M''(ω) shifts towards higher frequency, give rise decrease in τ_σ values of mixture while $\tau_\sigma$found to be highest 563ns for pure water and lowest 79.6 ns at f_σ= 2 MHz for 0.9989 mole fraction of water.

3.3 Complex conductivity:

The frequency dependent real part σ' and the imaginary part of σ'' of the alternating current (ac) complex conductivity σ*(ω) of the liquid samples were obtained from the following eq.3

$$\sigma^*(\omega) = \sigma' + j\sigma'' = \omega\varepsilon_0\varepsilon'' + j\varepsilon_0\varepsilon' \quad (3)$$

Where ε_0 is free space dielectric constant. Fig. 6 shows the σ'(ω) spectra for L-phenylalanine-water solution. Initially plot shows rapid increase in the conductivity thereafter all the concentration shows no effect of frequency on the σ_{ac}. Above such a frequency it is almost constant which corresponds to ionic or dc electrical conductivity. σ_{ac}found to be highest 0.011 S/m for mole fraction Xw = 0.9989 while lowest for water. For all other concentration it is between 0.0038 S/m and 0.0052 S/m.

3.4 Complex Impedance:

The complex impedance plane plots (Z'' vs. Z') are commonly used to separate the bulk material and the electrode surface phenomena. The frequency dependent values of the real part Z' and reactive part of Z'' of the complex impedance Z*(ω) of the liquids can be evaluated as

$$Z^*(\omega) = Z' - jZ'' = \left[\frac{R_P}{1+(\omega C_P R_P)^2} - j\frac{\omega C_P {R_P}^2}{1+(\omega C_P R_P)}\right]$$

Fig. 7 shows Z'' vs. Z' plots of aqueous L-phenylalanine. For all given concentration range, it exhibits two arcs: the low frequency arc suggests an electrode surface polarization effect whereas high frequency arc corresponds to the bulk material effect.

Conclusions:

The dielectric and electrical properties of aqueous L-phenylalanine have been studied between the frequency ranges of 2Hz to 2MHz. Various processes associated with the electrical and dielectric properties of aqueous solutions have been explained using dielectric parameters such as complex dielectric function ε*(ω), electrical modulus M*(ω), electrical conductivity σ*(ω) and complex impedance Z*(ω). The given data may be used to characterize pharmaceutical material using dielectric permittivity and conductivity and analyze pharmaceutical systems such as inter-batch variation, liposome suspensions, cyclodextrin etc.

Acknowledgements

Financial support provided by SERB, DST, New Delhi (SR/FTP/PS-203/2012) is gratefully acknowledged.

References:

[1] Milan Remko, Daniel Fitz, RiaBroer, Bernd Michael Rode, Journal of Molecular Modeling 17(2011) 3117.

[2] S. Tamilselvam, M. Vimalan, V. Potheher, S. Rajasekar, R. Jayasekaran, M. A. Arockiaraj, J. Madhavan, SpectrochimicaActa Part A: Molecular and Biomolecular Spectroscopy. 114(2013)19-26

[3] P. Jayprakash, M. P. Mohamed, P. Krishnan, M. Nageshwary, G. Mani, M. L. Caroline, Physica B: Physics of Condensed Matter. 503(2016) 25-31.

[4] SunithaNagaradona, RajanBabuDhanakotti, SpectrochimicaActa Part A: Molecular and Biomolecular Spectroscopy. 203(2018)147-157

[5] R. V. Femilaa, M. A. Raj, J. Madhavan, Materials Today: Proceedings. 8((2019)470-475

[6] K. Selvarani, R. Mahalakshmi, International Journal of ChemTech Research. 9(2016) 113-120

[7] M. Prakash, D.Geetha, M.L. Caroline, P. S. Ramesh, SpectrochimicaActa Part A: Molecular and Biomolecular Spectroscopy. 83(2011)461-466

[8] P. Sangeetha, P. Jayprakash, M. Nageshwary, M. P. Mohamed, G. Vinitha, M. L. Caroline, Chinese Journal of Physics= Taipei 56(2) 2018

[9] C. Peter A., Vimalan M., Sagayaraj P., Madhavan j., Physica B: Physics of Condensed Matter, 405(2010) 65-71.

[10] C.B. Silva, J. G. da Silva Filho, G. S. Pinheiro, A. M. R. Teixeira, P. T. Freire, Vibration Spectroscopy. 98(2018)128-133

[11] Y. S. Joshi, A. C. Kumbharkhane, Bionano Frontier. 8(2015)

[12] Y. S. Joshi, K. S. Kanse, A. C. Kumbharkhane, V. A. Rana, SRTMU Research Journal of Science.(2018) 10-15

[13] Y. S. Joshi, K. S. Kanse, D. N. Rander, A. C. Kumbharkhane, 54(2016)621-628

[14] S. B. Shinde, R. N. Mathpati, D. N. Rander, Y. S. Joshi, K. S Kanse, Printing Area: I. R. Journal. (2017) 97-101

[15] H. C. Chaudhary, A. Chaudhary, S. Mehrotra, Journal-Chinese Chemical Society Taipei. 52(1)2005

[16] Goeff Smith Alstair, P. Duffy, JieShen Cedric, J.Olliff, J. Pharmaceutical Sciences. 84 (1995) 1029-1044

[17] Duncan Q. M. Craig, Drug Development and Industrial Pharmacy. 18(2008)11-12

[18] Ciaran O. Fagain, Methods in Molecular Biology, Springer. 244(2004)

[19] Chaube H. A. &Rana, V. A. Solid State Phenomena 209 (2014) 182-185.

[20] Sengwa, R. J. &Sankhla, S. Colloid and Polymer Science (2007). 285, 1237-1246.

[21] Zhang, S., Dou, S., Colby, R. H. & Runt, J. J Non-cryst Solids (2005). 351, 2825-2830.

[22] Pradhan, D. K., Choudhary, R. N. P. &Samantaray, B. K. Express Polymers Letters (2008). 2, 630-638.

[23] Chanmal, C. V. & Jog, J. P. Express Polymer letters (2008). 2(4), 294-301.

Table 1
Mole fraction(Xw) of water Vs. Static dielectric constant(ε_0), Electrode polarization relaxation time(τ_{EP}), ionic conductivity relaxation time (τ_σ) Refractive index and density of aqueous L-Phenylalanine at 25^0C.

Xw	ε_0	τ_{EP}(μs)	τ_σ (ns)
1.0000	78.71	50.20	563
0.9994	79.45	14.96	149

0.9989	79.95	5.63	79.6
0.9983	80.80	15.87	178
0.9979	80.56	11.91	141
0.9972	82.27	12.61	158

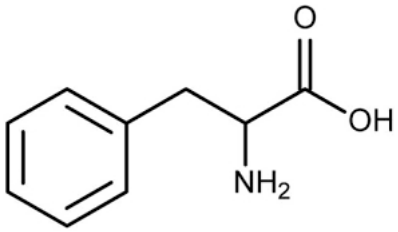

Fig.1. Molecular structure of L-phenylalanine

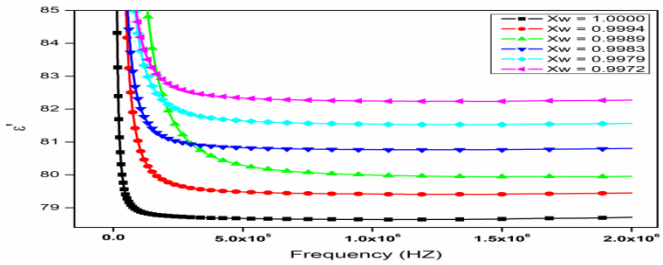

Fig.2. Frequency dependent spectra of the real part of the relative dielectric function ε' for aqueous L-phenylalanine.

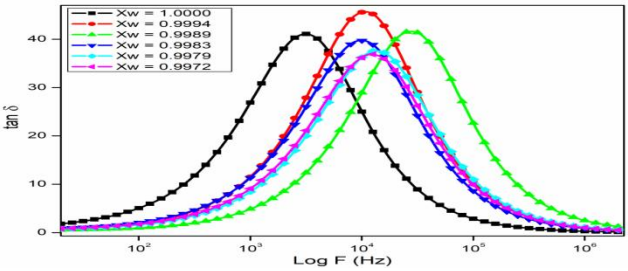

Fig.3. Frequency dependent spectra of dielectric loss tangent (tan δ) for aqueous L-phenylalanine.

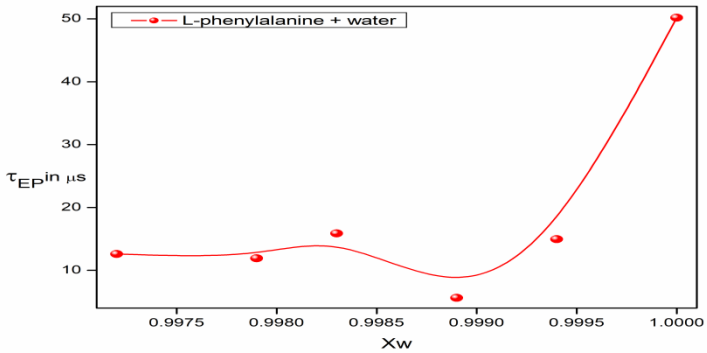

Fig. 4. The electrode polarization relaxation time ($\boldsymbol{\tau}_{EP}$)for aqueous L-phenylalanine.

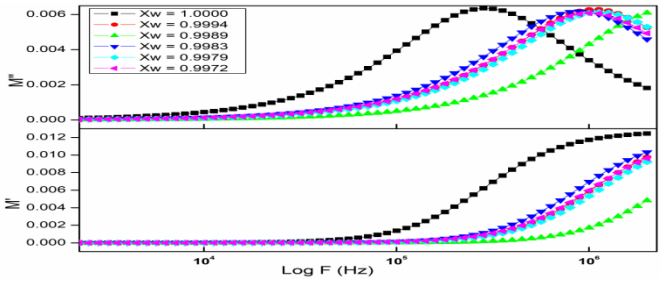

Fig.5. Real part (M') and imaginary part (M'') of the complex electric modulus [M*(ω)] for aqueous L-phenylalnaine.

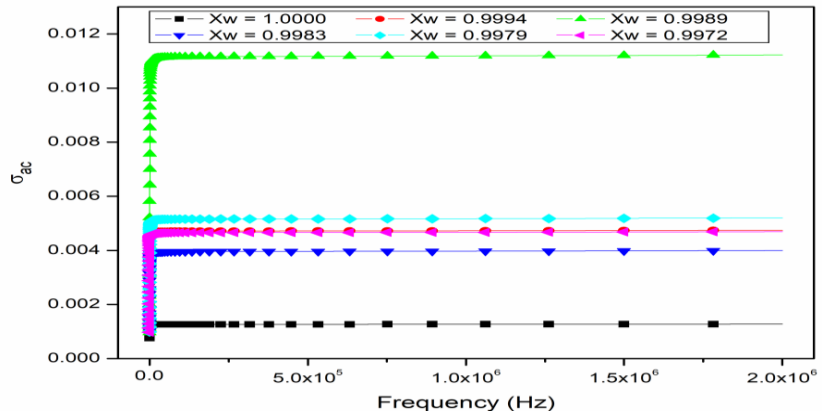

Fig.6. Theσ' (ω) spectra for aqueous L-phenylalanine.

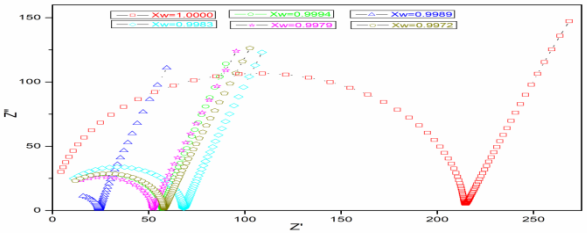

Fig.7. Complex impedance plot Z' vs. Z'' for aqueous L-phenylalanine.

Paper 45

Synthesis and Characterization of Bismuth Ferrite (BFO) Prepared by Auto Combustion Method for Photovoltaic Application

Sagar Pardhi[a], Milind Bhandare[a,] Madhav Sarode [b,*]

[a] *Department of Physics, Mahatma Phule Mahavidyalaya Pimpri, Pune, MS, India*

[a] *Department of Physics, Mahatma Phule Mahavidyalaya Pimpri, Pune, MS, India*

[b]*Department of Physics, Rayat Shikshan Sansth's Radhabai Kale Mahila Mahavidyalaya, Ahmednagar, MS, India.*

Abstract

Herein, we report synthesis and characterization of Bismuth Ferrite (BFO) prepared by Auto Combustion Method. $BiFeO_3$ based materials are currently one of the most studied multiferroics due to their possible applications at room temperature. Multiferroic bismuth ferrite were synthesized using the auto-combustion method. The structural and optical properties were investigated in detail. X-ray diffraction results confirm the formation of BiFeO3 as a major phase with a small number of impurity phases, which will be subsequently removed by adding the dilute nitric acid. X-ray diffraction pattern shows crystalline nature. The average crystallite size was found to be 66nm. In the case of UV-visible absorption spectroscopy (UV-VIS) maximum absorption wavelength of the hump is found to be 308nm. The structural and optical properties of the prepared material have been investigated. The band gap values of found to be 2.7 eV, which will be useful for photovoltaic applications. In addition to this, the spectroscopic diagnosis is carried out with help of the FTIR technique. The absorption peak at 830 cm^{-1} indicates that the crystalline phase of pure BFO.

Keywords: Bismuth Ferrite (BFO); Optical properties, Auto-combustion method.

* Corresponding author: sarodemadhav@gmail.com

---

1. Introduction

Multiferroic nanomaterials are materials that can possess several properties like Ferro electricity, ferromagnetism and Ferro elasticity in a single crystal [1-6]. Multiferroic materials have recently attracted a great deal of interest due to the coexistence of different order parameters in a crystalline phase. Thus, it has broad applications in multifunctional, low-power consumption, and environmentally friendly devices [4, 7, 8]. Bismuth ferrite ($BiFeO_3$) has been found to have a ferroelectric phase transition Curie temperature (TC) of 1103 K and a G-type

antiferromagnetic phase transition Neel temperature (TN) of 643 K, which are much higher than room temperature [9]. Due to the high TC and TN, BFO becomes the most promising and widely known multiferroic material [7, 9].

Since it is difficult to synthesize BFO without impurity phases. Due to the large surface area and various morphologies, BFO nanostructures exhibit significantly enhanced visible-light photocatalytic ability and magnetization. Moreover, with a low band gap, BFO-based nanomaterials present a strong photovoltaic effect. Because of the remarkable multifunctional properties, BFO-based nanomaterials have attracted great research enthusiasm in recent years. Furthermore, the research enthusiasm will continue in the future.

S. R. Dhanya et al synthesised $BiFeO_3$ powder and studies spectroscopic characteristics and he concluded that sintering temperature of 820^0C is best suited for BFO synthesis [10].M. Muneeswaran et al synthesised nanosized $BiFeO_3$ powder whose FT-IR spectra revealed that absorption bands at 555 and 445 cm-1 are due to the stretching vibration of Fe-O and the bending vibration of O-Fe-O bond respectively [11]. Wei Cai et al studied ferroelectric property and band gap in Ti-doped bismuth ferrite and found the band gap of pure BFO is 2.58 eV[12].

In the present communication, we synthesised pure BFO which have focused on the structural and optical properties for photovoltaic application.

2. Experimental procedure:

Bismuth ferrite powder was synthesized by a solution evaporation route. 0.25 M Bi $(NO_3)_3$ and 0.25 M Fe $(NO_3)_3$ solution prepared by dissolving in dilute nitric acid. These two solutions were mixed in a beaker. To this Glycine with mole ratio 0.1 concerning nitrate was added to the above solution. The surfactant added was with a mole ratio of 0.05 with respect to metal. The surfactant used Triton X. This solution was heated on a hot plate under the continuous stirring condition to its boiling temperature until all the liquid evaporated. There was an immense evolution of brown fumes, towards the end of the reaction. A fluffy brown mass was obtained at the base of the beaker. Then the powder was sintered at 700°C for 4 hours.

3. Result and discussion

3.1. Structural Properties:

Fig. 1 shows the XRD patterns of BFO powder sintered at a temperature of 700^0C for 4 hr.

From fig.1 it clear that, all the diffraction peaks in the XRD pattern can be indexed as a pure phase of BFO with Rhombohedral distorted Peroskites structure belonging to the R3c space group. Few second phase impurity peaks attributed to Bi or Fe rich phases, i.e $Bi_2Fe_4O_9$ and

$Bi_{25}FeO_4$ has been reported by several authors [13-14]. The average crystallite size was calculated from (110) peak (at 2θ= 33.12) by using Scherer's formula

$$D = \frac{(0.9)\lambda}{\beta\ Cos\theta}$$

Where,

D = The average crystallite size

λ = X-ray wavelength

β = full width at half maximum intensity (FWHM)

θ = the angle of diffraction

The average crystal size is found to be 66 nm.

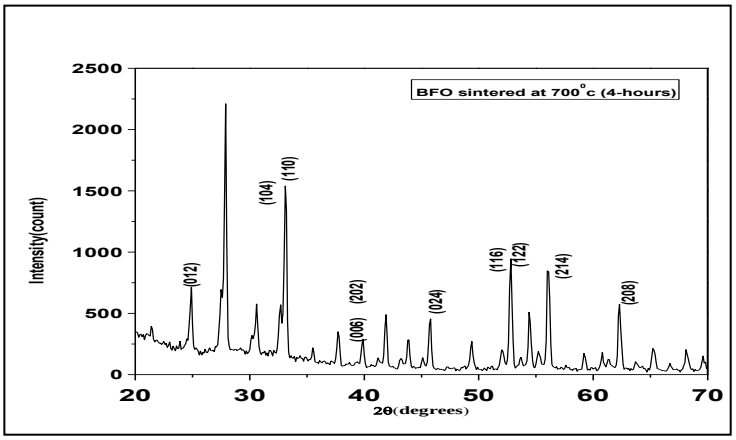

Fig.1: XRD Pattern of BFO sintered at a temperature of 700^0C.

The lattice parameters as shown in table-1 are in good agreement with those obtained from pure phase BFO prepared by ceramic and solid-state reaction [15]. Similar results were obtained by Ashish Gautam and his Co-workers [14].

TABLE 1. Lattice parameters of BFO sintered at 700^0C

Parameter	Value
a	4.5294 (A^0)
c	13.5800 (A^0)
Cell volume	171.85
Distortion value (c/a)	2.9981 (A^0)

3.2. Optical Properties:

Absorbance characteristics can be used to determine photo-catalytic activity in the decomposition of organic compounds. The UV–Vis absorbance spectrum of sintered BFO at

700^0C for 4 hrs as shown in fig.2 (a). Generally, UV–Vis absorbance spectra of BFO have a strong region in 300–550 nm and slight absorption in 550–700 nm. In our case absorption edge is obtained at 306 nm. The band gap energy range play important role in the application of bismuth ferrite for making promising materials.

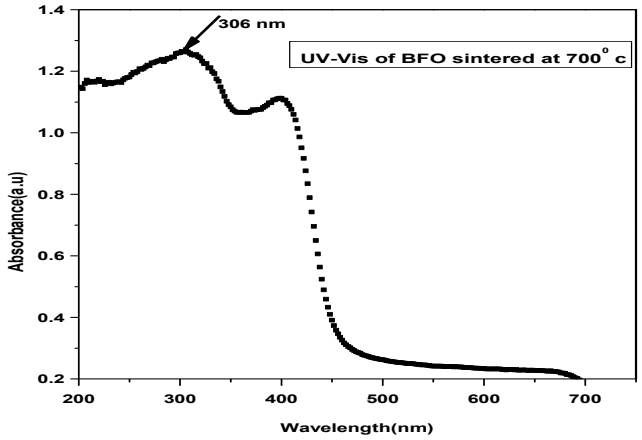

Fig.2 (a) UV-Visible Spectra of BFO sintered at a temperature of 700^0C

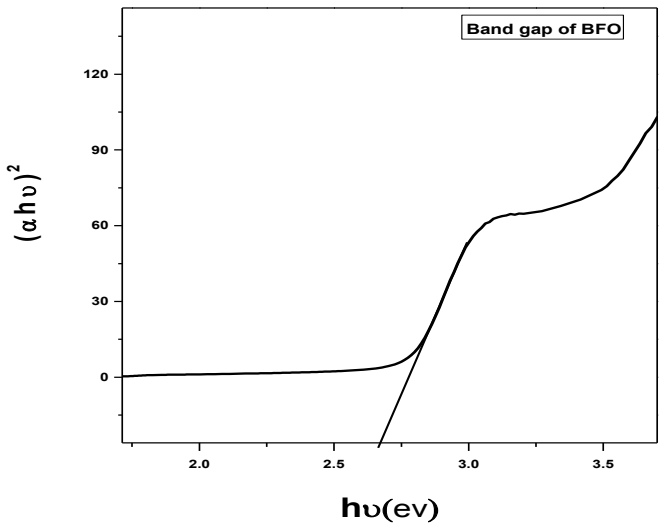

Fig. 2 (b) Variation of $(\alpha h\upsilon)^2$ vs $h\upsilon$

The values for optical band gaps (E_g) are obtained by using Tauc's plots. The UV–Visible spectra (Fig. 2 (a)) are used to generate the Tauc's plots defined by using equation:

$$(\alpha h\upsilon)^n = A\,(h\upsilon - E_g)$$

where α is a absorption coefficient, A is a constant independent of photon energy, hυ is the photon energy and n is a constant equal to 2 for direct allowed transitions.

The direct band gap can be calculated with help of a fig.2 (b) which shows $(\alpha h\upsilon)^2$ vs $h\upsilon$ plot. The value of Eg is obtained by extrapolation of the straight-line intercept at the horizontal axis portion of the plot to zero absorption edge in a graph of $(\alpha h\upsilon)^2$ vs $h\upsilon$ as shown in fig. 2 (b). As BFO is a direct band gap semiconductor, the value of the direct energy band gap are found to be 2.7 eV. The band gap value in our case is comparable with the earlier reported values [16]. In recent years, the photovoltaic characteristics of BFO have gained wide attention because of its narrow band gap (2.3–2.7 eV) [17-24]. Therefore, a low band gap of BFO is used for Photo-catalysis in degradation applications.

3.3. Molecular bonding:

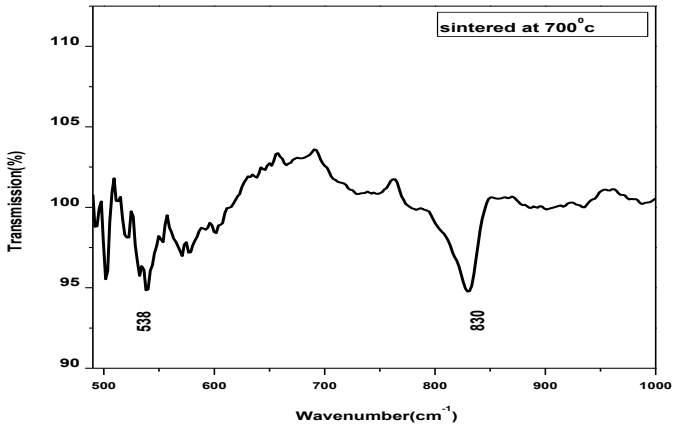

Fig.3. FT-IR Spectrum of BFO sintered at 700^{0}C for 4 hrs.

To study the molecular bonding in a material FT-IR analysis is used. The vibrational frequency of atomic bonds contains peaks that help to identify the bonds present in a material. Fig.(3) shows the FTIR plot of the BFO sample prepared by the Auto combustion Method. The peaks obtained at the position of 538 cm^{-1} are due to the stretching vibrations of the Metal oxygen (Fe-O) [10]. Fe-O absorption peak at 830 cm^{-1} is due to the high crystalline phase of pure BFO. The metal-oxygen bonds confirm the formation of the Perovskite structure. The vibrational frequency is determined by following the equation for the Fe-O bond

$$\nu = \frac{1}{2\pi c}\sqrt{\frac{k}{\mu}}$$

The relation between force constant (k) and average Fe-O bond length(r) is k-17/r^3 as shown in table 2, the types of vibrations responsible for BFO giving rise to the FTIR spectrum is tabulated.

Table 2. FTIR details of BFO Functional group Type of vibration Characteristic Absorptions (cm^{-1}) Intensity.

C-Br	Stretching at 500-600	strong
C-O	Stretching at 675-1000	strong

The values of wave number, Effective Mass, Force Constant and Bond length of BFO sintered at 700^{c} C for 4hrs are given in table 3.

Table 3: Effective Mass, Force Constant and Bond length of BFO sintered at 700^{c} C

Composition	Wave number	Effective mass	Force constant	Fe-O Bond length
BFO sintered at 700^{0}C	540	2.064	2.1204 N/cm	2.001

Conclusions:

Single-phase BFO Perovskite crystallites have been prepared from bismuth and iron nitrates by using the Auto-combustion method. XRD pattern indicates that the crystalline structure of BFO is formed at sintering temperature 700^{0} C with a small impurity phase. Crystalline size is found in nanosized. In absorption spectra, Hump is obtained at 306 nm and the value of the direct energy band gap is 2.7 eV. It will be useful for photovoltaic applications. The absorption peak at 830 cm^{-1} indicates that the crystalline phase of pure BFO.

Acknowledgement

The authors are grateful to acknowledge the Department of Physics Mahatma Phule Mahavidyalaya Pimpri . This work was supported by Mahatma Phule Mahavidyalaya Pimpri, under DST-FIST grant.

Referance:-

1. G. Catalan, J.F. Scott, Physics and applications of bismuth ferrite. Adv. Mater. 21, 2463–2485 (2009).
2. S.-W. Cheong, M. Mostovoy, Multiferroics: a magnetic twist for ferroelectricity. Nat. Mater. 6, 13–20 (2007).
3. N. Hur, S. Park, P.A. Sharma, J.S. Ahn, S. Guha, S.W. Cheong, Electric polarization reversal and memory in a multiferroic material induced by magnetic felds. Nature 429, 392–395 (2004).

4. R. Ramesh, N.A. Spaldin, Multiferroics: progress and prospects in thin flms. Nat. Mater. 6, 21–29 (2007).
5. J.F. Scott, Multiferroic memories. Nat. Mater. 6, 256–257 (2007).
6. S. Seki, X.Z. Yu, S. Ishiwata, Y. Tokura, Observation of skyrmions in a multiferroic material. Science 336, 198–201 (2012).
7. J. Wang, J.B. Neaton, H. Zheng, V. Nagarajan, S.B. Ogale et al, Epitaxial BiFeO3 multiferroic thin film Nano-Micro Lett. (2020) 12:81 Page 19 of 23 81 1 3 heterostructures. Science 299, 1719–1722 (2003).
8. N.A. Spaldin, M. Fiebig, The renaissance of magnetoelec- tric multiferroics. Science 309, 391–392 (2005).
9. J.C. Yang, Q. He, P. Yu, Y.H. Chu, BiFeO3 thin flms: a play- ground for exploring electric-feld control of multifunction- alities. Ann. Rev. Mater. Res. 45, 249–275 (2015).
10. S. R. Dhanya, Soumya G. Nair, Jyotirmayee Satapathy, N. Pavan Kumar, et al. "structural and spectroscopic characterization of bismuth- ferrite"AIP Conference Proceeding 25 october 2019 (1-8)
11. M. Muneeswaran, P. Jagatheesan and N.V. Giridharan, "Synthesis of nanosized BiFeO3 powders by Co-precipitation method", Journal of Experimental Nanosscience, Vol.8, 2013, 341-346.].
12. Wei Cai, Chunlin Fu, Rongli Gao, Weihai Jiang, Xiaoling Deng, Gang Chen, "Photovoltaic enhancement based on improvement of ferroelectric property and band gap in Ti-doped bismuth ferrite thin films" Journal of Alloys and Compounds 617(2014) 240-246).
13. Karimi S, Reaney IM, Han Y, Pokorny J, Sterianou IJ. Mater Sci 2009;44:5102
14. Ashish Gautam a, K. Singh a , K. Sen a , R.K. Kotnala b , M. Singh Mater Lett 65 2011 591-594
15. Mukasyan AS, Dinka P. Int J Self Propag High Temp Synth (2007)16-23;
16. S.J. Clark, J. Robertson, Applied Physics Letters 94/2 (2009) 022902]
17. W.M. Lee, J.H. Sung, K. Chu, X. Moya, D. Lee, C.J. Kim, N.D. Mathur, S.W. Cheong, C.H. Yang, M.H. Jo, Adv. Mater. 24 (2012) OP49–OP53.
18. M. Alexe, Nano. Lett. 12 (2012) 2193–2198.
19. H.W. Chang, F.T. Yuan, Y.C. Yu, P.C. Chen, C.R. Wang, C.S. Tu, S.U. Jen, J. Alloys Comp. 574 (2013) 402–406.

20. J.H. Sung, W.M. Lee, J.H. Lee, K. Chu, D. Lee, X. Moya, N.D. Mathur, C.H. Yang, J.H. Park, M.H. Jo, NPG Asia Mater. 5 (2013) e38.
21. Z.B. Lin, W. Cai, W.H. Jiang, C.L. Fu, C. Li, Y.X. Song, Ceram. Int. 39 (2013) 8729–8736.
22. C.M. Hung, C.S. Tu, Z.R. Xu, L.Y. Chang, V.H. Schmidt, R.R. Chien, W.C. Chang, J. Appl. Phys. 115 (2014) 17D901.
23. L. Fang, L. You, Y. Zhou, P. Ren, Z.S. Lim, J.L. Wang, Appl. Phys. Lett. 104 (2014) 142903.
24. V.S. Puli, D.K. Pradhan, R.K. Katiyar, I. Coondoo, N. Panwar, P. Misra, D.B. Chrisey, J.F. Scott, R.S. Katiyar, J. Phys. D: Appl. Phys. 47 (2014) 075502.

Paper 46

Comparative studies of SHG efficiency of L-Alanine and Glycine doped BisThiourea Cadmium Chloride (BTCC) single crystal

Dhumane N. R.

Shri Anand College, Pathardi Dist.-Ahmednagar (M.S.)

Abstract:

Bisthiourea cadmium chloride (BTCC) is promising semi organic nonlinear optical material from metal complexes of thiourea. BTCC is a potential NLO material for various applications in the field of laser and optoelectronics. In present investigation L-Alanine and Glycine were in mole % in saturated solution of BTCC in order to increase SHG efficiency. The effect of L-Alanine and Glycine on SHG efficiency was studied by Kurtz and Perry powder test. The L-Alanine and Glycine doped BTCC crystals were grown from aqueous solution by slow evaporation. The Grown crystals were subjected for different characterization. The FTIR spectroscopy studies were used to analyze qualitatively the presence of functional groups in synthesized compound. The effect of L-Alanine and Glycine on transmittance of grown crystals were studied by UV-visible spectroscopy. The crystal structure was confirmed by single crystal X-ray diffraction.

Keywords: SHG, BTCC, Glycine, L-Alanine, etc..

Introduction:

In recent years the researchers have been working to develop new inorganic, organic, and semi-organic nonlinear optical (NLO) crystals [1, 2]. The material selection is influenced not only by laser conditions, but also by the physical properties of the grown crystal, such as transparency, damage threshold, conversion efficiency, phase matching, and temperature stability [3, 4]. Materials with increased second order nonlinearities, a large optical transmission window, and stable physicochemical performance are required for several applications and optical storage devices [5].There has been a considerable interest in the synthesis of semi organic NLO materials with excellent second order optical nonlinearities in recent years [6-8].Semi organic nonlinear optical crystals combine good thermal and mechanical properties of inorganic compound with high optical nonlinearity of purely organic compound [9-11].In case of metal–organic coordination complexes, the organic ligand is usually more dominant in the NLO effect. Since metal compounds have a high transparency in the UV region (because of their closed d10 shell), there has been

focused on the group (IIB) metals such as Zn, Cd and Hg [12]. Among organic NLO materials, thiourea molecules coordinate with several metal complexes to produce NLO materials. Recently metal complexes of thiourea have emerged as a strong second order nonlinear optical materials for laser applications [13, 14].

Bis thiourea cadmium chloride (BTCC) is a potential NLO material from metal complexes of thiourea. BTCC is 0.73 times more nonlinear than urea [14]. At higher frequencies BTCC has very low dielectric constant [15]. It also possesses high laser damage threshold and good mechanical properties [16]. The effects of several dopants on structural and physical properties of metal complexes of thiourea and KDP have been reported [17]. Semi-organic nonlinear optical (NLO) crystals formed by amino acids with inorganic materials possess the advantages of high optical nonlinearity of the organic amino acids. Most of the amino acid itself exhibits nonlinear optical properties due to donor amino group NH3+ and acceptor carboxyl group COO- and intermolecular charge transfer is also possible [18]. Therefore, amino acids can be used as dopants and it was observed that there is enhancement in the material properties such as nonlinear optical (NLO) and ferroelectric properties [19].Amino acid in solution at neutral pH has zwitterions rather than unionized molecules [18].

Experimental

Synthesis and Crystal Growth

BisThiourea Cadmium Chloride (BTCC) was synthesized by dissolving two mole of AR grade thiourea with one mole of cadmium chloride in excess water. The solution was slowly evaporated until solvent completely dried and white crystalline salt was obtained. Purity of synthesized salt was increased by successive recrystallization process before the actual experiments.

Saturated solution of BTCC was prepared in six different beakers and 1, 2 and 3mole% L-Alanine and Glycine were added in these six beakers. The salts were obtained by slow evaporation of solutions. The obtained salts were purified by recrystallization process and tested for SHG by Kurtz and Perry powder SHG test.The SHG efficiency of 1mole% L-Alanine and 2mole% glycine doped BTCC was found to be higher than other concentrations and pure BTCC. Hence 1mole% L-Alanine doped BTCC and 2mole% glycine doped BTCC single crystals were grown by slow evaporation technique in a constant temperature bath controlled to an accuracy of ±0.01˚C.

Result and Discussion

1. **SHG Measurement**

The initial testing of materials for second harmonic generation was carried out by classical powder method developed by Kurtz and Perry [20]. It is an important and popular tool to evaluate the conversion efficiency of NLO materials. The fundamental beam of 1064 nm from Q switched Nd: YAG laser was used to test the Second Harmonic Generation (SHG) property of 1, 2 and 3mole% L-Alanine and Glycine doped BTCC and pure BTCC. Pulse energy 3 mJ/pulse and pulse width 8ns and repetition rate 10 Hz was used. The photo multiplier tube (Hamahatsu R2059) was used as detector and 90 degree geometry was employed. The input laser beam was passed through an IR detector and then directed on the microcrystalline powdered sample packed in a capillary tube of diameter 0.154 mm. The assembly of an oscilloscope and photodiode detector is employed to measure the light emitted by the sample. The SHG signal generated in the sample was confirmed from emission of green radiation from the sample. The SHG conversion efficiency of L-Alanine and Glycine doped BTCC was found to be enhanced than that of pure BTCC. The optical signal generated from sample was converted in to electrical signal and measured on oscilloscope. The output for pure BTCC, 1, 2 and 3mole% L-Alanine doped BTCC and 1, 2 and 3mole% Glycine doped BTCC was measured. The SHG conversion efficiency of 1mole% L-Alanine doped BTCC and 2mole% glycine doped BTCC is greater than pure BTCC and other molar concentrations of L-Alanine and Glycine in BTCC. The measured SHG efficiency is **1.124** times for 1mole% L-Alanine doped BTCC crystal and is **1.12** times for 2mole% Glycine doped BTCC than pure BTCC.

2. Single crystal X-ray Diffraction

To determine crystal structure and lattice parameter, grown crystal was characterize by single crystal X-ray diffraction technique by using BrukerAxs (Kappa Apex2) diffractometer. Observed values of lattice parameters for 1 mole% L-Alanine doped BTCC are a = 5.824 Å, b = 6.483 Å, c = 13.124 Å with volume 495.50 $Å^3$ and $\alpha = \beta = \gamma = 90^\circ$ and 2 mole% Glycine doped BTCC are a = 5.826 Å, b = 6.491 Å, c = 13.104 Å and $\alpha = \beta = \gamma = 90^\circ$ and volume 495.54 $Å^3$ This confirms that the both the crystals belongs to orthorhombic system and space group $Pmn2_1$. The observed values of lattice parameter agree with the reported values [13, 21].

3. Fourier Transform Infrared Spectroscopy (FTIR) Analysis

The FTIR spectroscopy studies were used to analyze qualitatively the presence of functional groups in synthesized compound. The FTIR spectrums of pure BTCC and 1 mole% L-Alanine and 2 mole% Glycine doped BTCC were recorded using Perkin Elmer Spectrum FTIR spectrometer by KBr pallet technique in the range 450-4000cm-1 and shown in Fig. 1, Fig. 2 and Fig. 3

respectively. The characteristic vibrational frequencies of the functional groups of 1 mole% L-Alanine and 2 mole% Glycine doped BTCC have been compared with pure BTCC and thiourea [18, 27, 28]. The comparison of characteristic vibrational frequencies has been tabulated in Table 1. The comparison shows slight shift in characteristics vibrational frequencies of 1 mole% L-Alanine and 2 mole% Glycine doped BTCC with respect to pure BTCC. This confirms the addition of L-Alanine and Glycine in grown crystal.

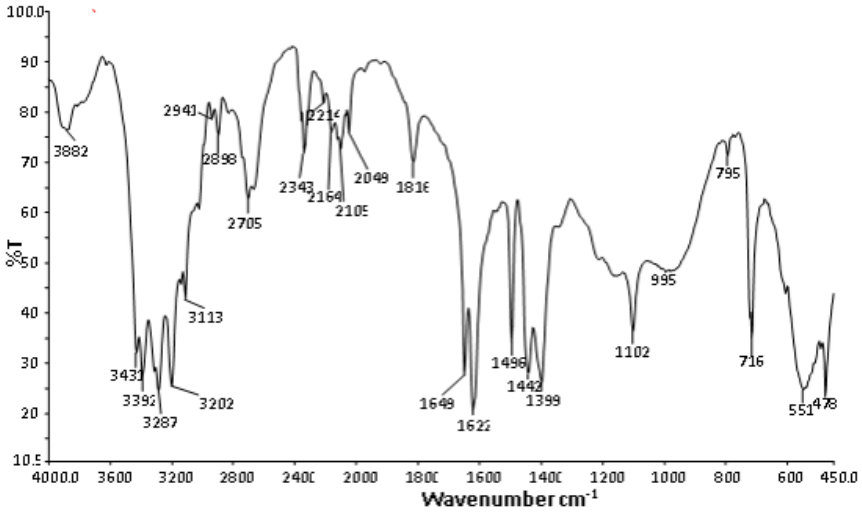

Fig. 1. FTIR spectra of pure BTCC

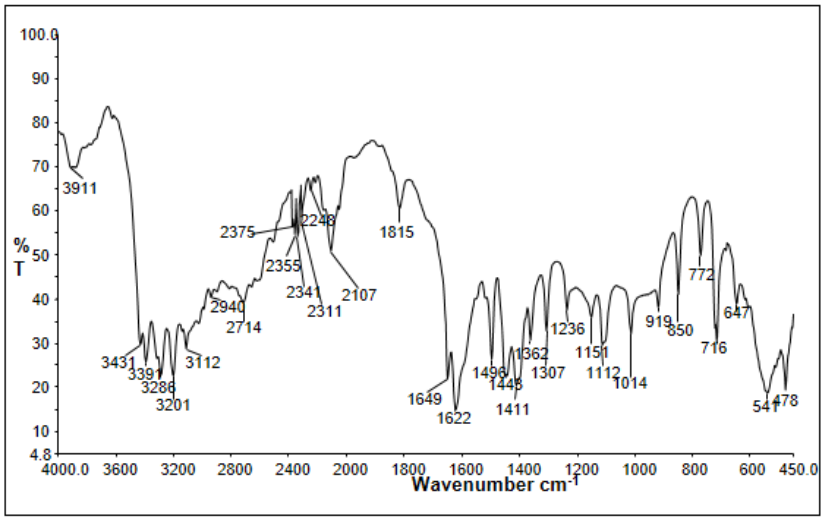

Fig. 2. FTIR spectra of 1 mole% L-Alanine doped BTCC

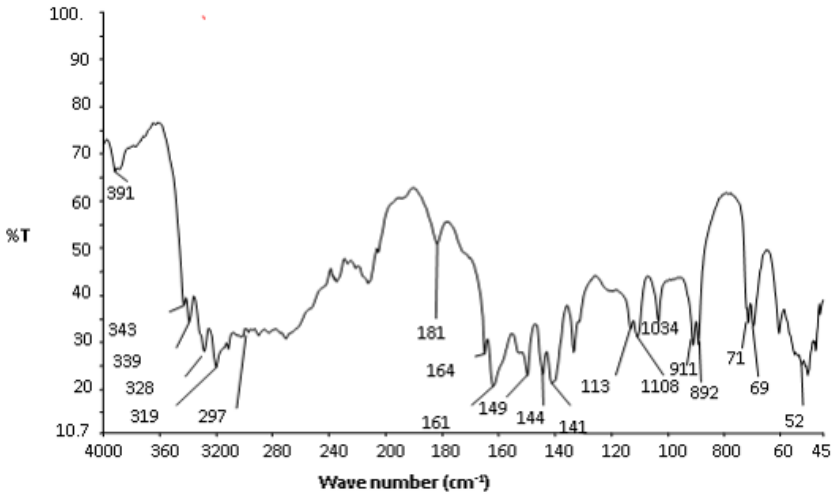

Fig. 3. FTIR spectra of 2 mole% Glycine doped BTCC

Table 1. Comparison of IR bands of 1 mole% L-Alanine and 2 mole% Glycine doped BTCC with thiourea and pure BTCC.

Thiourea	BTCC	1mole% L-Alanine doped BTCC	2mole% Glycine doped BTCC	Assignment
411	--	--	-	δs(N-C-N)
469	478	478	-	δs(S-C-N)
494	551	541	527	δas(N-C-N)
740	716	716	699	vs(C=S)
		772	716	vs(C=S)
1089	1102	1112	1108	vs(C-N)
		1151	1132	vs(C-N)
1417	1399	1411	1410	vas(C=S)
--	1442	1443	1443	vas(C-N)
	1496	1496	1497	v(N-C-N)
1627	1622	1622	1619	$\delta(NH_2)$
	1649	1649	1649	$\delta(NH_2)$
	1816	1815	1817	$\delta(NH_2)$
	2941	2940	2971	$\delta(NH_2)$

3167	3202	3201	3199	vs(NH_2)
3280	3287	3286	3284	vs(NH_2)
3376	3392	3391	3391	vas(NH_2)
	3431	3431	3430	vas(NH_2)

δ – bending, v – stretching, s – symmetric, as – asymmetric.

4. UV-visible Spectral Study

5. The UV–vis. studies of the grown crystal were carried out by Shimadzu UV 1600 UV-vis. spectrometer in a range 190-1100 nm. The absorption spectra of 1mole% L-Alanine and 2 mole% Glycine doped BTCC is shown in Fig. 4 and Fig. 5 respectively. The window shown in figure shows the absorption spectra of pure BTCC for comparison. The absorption spectra shows lower cutoff wavelength at around 283nm for L-Alanine doped BTCC and below 300nm for Glycine doped BTCC. From comparison of both spectra, it is obvious that there is no change in transparency region due to addition of L-Alanine and Glycine in BTCC. The absorption in the near UV region arises from electronic transitions associated within thiourea units of BTCC. The π- orbital electron delocalization in thiourea arises from mesomeric effect is responsible for the absorption near UV region. Thus the grown crystals have wide range of transparency in UV, visible and IR region. Hence the grown crystals are potential candidates for NLO applications.

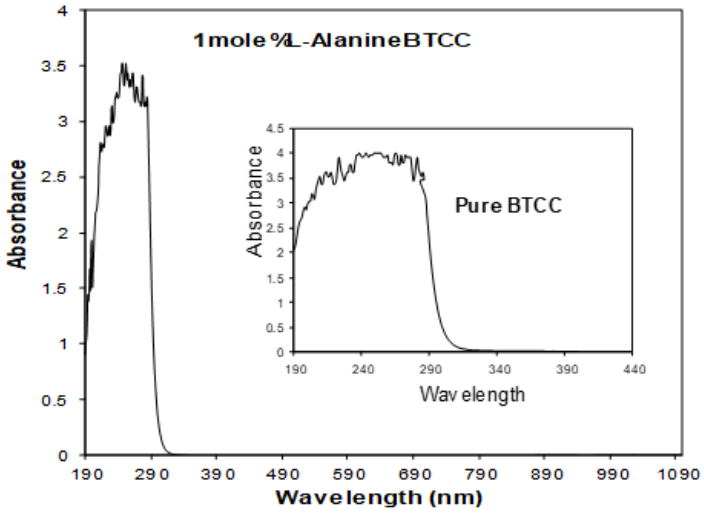

Fig. 4. UV-visible spectrum of 1mole% L-Alanine doped BTCC

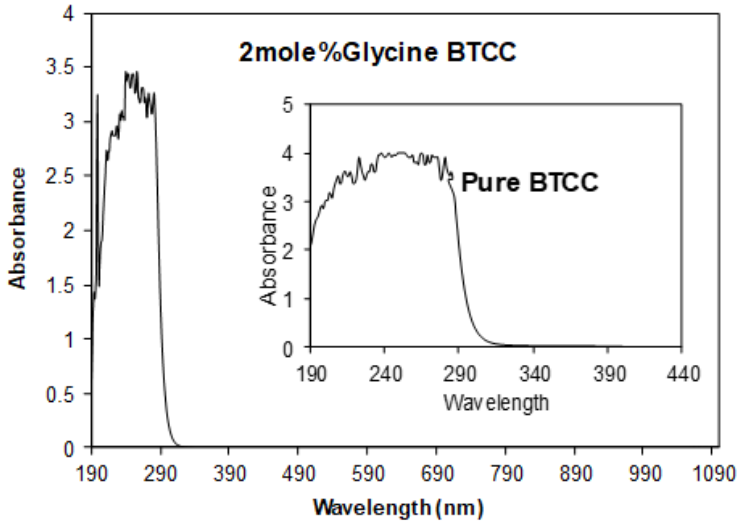

Fig. 5. UV-visible spectrum of 2mole% Glycine doped BTCC

Conclusion

The 1 mole% L-Alanine and 2 mole% Glycine doped BTCC crystals were grown by low temperature solution growth, slow evaporation technique. The Kurtz and Perry powder SHG test shows higher enhancement for 1 mole% L-Alanine and 2 mole% doped BTCC. The SHG efficiency of 1mole% L-Alanine doped BTCC is **1.124** and 2 mole% Glycine doped BTCC is **1.12** times more than pure BTCC. The L-Alanine has additional methyl group than Glycine which is responsible to produce large non-Centro symmetry than Glycine at lower doping concentration. Thus the enhancement in SHG efficiency for L-Alanine doped BTCC is observed at lower concentration than Glycine. Single crystal X-ray diffraction analysis confirms orthorhombic structures of the grown crystals. The presence of all the functional groups was confirmed by FTIR analysis. The UV-visible absorption spectra shows lower cutoff wavelength at around 300 nm and crystal has wide range of transparency in UV, visible and IR region. Thus the grown crystals are potential candidate for optoelectronic and laser applications.

References

1. S SHussaini, N R Dhumane, G Rabbani, P Karmuse, V G Dongre, M D Shirsat. “Growth and high frequency dielectric study of pure and thiourea doped KDP crystals”, Cryst Res Technol**42** (2007) 1110.

2. S SHussaini, N R Dhumane, V G Dongre, P Karmuse, P Ghughare, M D Shirsat. “Effect of glycine on the optical properties of zinc thiourea chloride (ZTC) single crystal”, Opt Elect Adv Mat. (Rapid Commun.) **2** (2008) 108.
3. R MohanKumar, D RajanBabu, D Jayaraman, R Jayaval, K Kitmura. “Studies on the growth aspects of semiorganic L-alanine acetate: a promissing NLO crystal”, J Cryst Growth **275** (2005) e1935.
4. D PremAnand, M Gulam Mohamed, S A Rajasekar, S Selvakumar, A Joseph Arul Pragasam, P Sagayaraj. “Growth and characterization of pure, benzophenone and iodine doped benzoyl glycine single crystals”, Mater ChemPhys**97** (2006) 501.
5. X Q Wang, D Xu, M K Lu, D R Yuan, J Huang, S G Li, G W Lu, HQ Sun, S Y Guo, G H Zhang, X L Duan, H Y Liu, W L Liu. “Physicochemical behavior of nonlinear optical crystal $CdHg(SCN)_4$”, J Cryst Growth **247** (2003) 432.
6. K Ambujam, K Rajarajan, S Selvakumar, Vetha I Pothekar, A Ginson Joseph, P Sagayaraj. “Growth and characterization of a novel NLO crystal bis-glycine hydrogen chloride (BGHC)”, J Cryst Growth **286** (2006) 440.
7. S S Hussaini, N R Dhumane, V G Dongre, P Karmuse, P Ghughare, M D Shirsat. “Effect of glycine on the optical properties of zinc thiourea chloride (ZTC) single crystal”, Opt Elect Adv Mater (Rapid Commu) **2** (2008) 108.
8. S SHussaini, N R Dhumane, V G Dongre, P Karmuse, P Ghughare, M D Shirsat. “Growth and characterization of glycine doped KDP single crystal for optoelectronic applications”, Opt Elect Adv Mater (Rapid Commu) **1** (2007) 707.
9. Min-Hua Jiang, Qi Fang. “Organic and semiorganic NLO materials”, Adv Mater **11** (1999) 1147.
10. P M Ushasree, R Muralidharan, R Jayavel, P Ramasamy. “Growth of bis (Thiourea) cadmium chloride single crystals- a potential NLO material of organometallic complex”, J Cryst Growth **218** (2000) 365.
11. S Dhanuskodi, K Vasantha, P A Angeli Mary. “Structural and thermal characterization of a semiorganic NLO material: l-alanine cadmium chloride”,SpectroActa Part A**66** (2007) 637.

12. H Q Sun, D R Yuan, X Q Wang, X F Cheng, C R Gong, M Zhou, H Y Xu, X C Wei, C N Luan, D Y Pan, Z F Li, X Z Shi. "A novel metal-organic coordination complex crystal: tri-allythiourea zinc chloride (ATZC)", Cryst Res Technol**40** (2005) 882.
13. V Kannan, N P Rajesh, R Bairava Ganesh, P Ramasamy. "Growth and characterization of Bisthiourea Zinc Acetate, a new nonlinear optical material", JCryst Growth **269**(2004) 565.
14. A Pricilla Jeyakumari, J Ramajothi, S Dhanuskodi."Structural and microhardnessstudies of NLO material – bisthiourea cadmium chloride", J Cryst Growth **269**(2004) 558.
15. N R Dhumane, S S Hussaini, V V Nawarkhele, M D Shirsat. "Dielectric studies of metal complexes of thiourea crystals for electro-optic modulation", Cryst Res Technol**41** (2006) 897.
16. S Selvakumar, J Packiam Julius, S A Rajasekar, A Ramanand, P Sagayaraj. "Microhardness, FTIR and transmission spectral studies of Mg^{2+} and Zn^{2+} doped nonlinear optical BTCC single crystals", Mater Chem Phys**89** (2005) 244.
17. V Kannan, R Bairava Ganesh, R Sathyalakshmi, N P Rajesh, P Ramasamy. "Influence of La^{3+} ions on growth and NLO properties of KDP single crystals", Cryst Res Technol**41** (2006) 678.
18. LubertStryer, "Biochemistry" W. H. Freeman and Company, New York (1995) Forth Edition.
19. S SHussaini, N R Dhumane, V G Dongre, P Karmuse, P Ghughare, M D Shirsat. "Growth and characterization of glycine doped KDP single crystal for optoelectronic applications", Opt Elect Adv Mat (Rapid Commun.) **1** (2007) 707.
20. S K Kurtz and T T Perry. "A powder technique for the evaluation of nonlinear optical materials", J ApplPhys**39** (1968) 3798.
21. J Ramajothi, S Dhanuskodi, K Nagarajan. "Crystal growth, thermal, optical and microhardness studies of tris (thiourea) zinc sulfate- a semiorganic NLO material", Cryst Res Technol**39** (2004) 414.

Paper 47

DEVELOPMENT OF MULTIGRAIN INSTANT PORRIDGE

Bagade Aditi J.[1]

Temkar Vaishnavi S.[2]

Suse Sachin N.[3]

[1.2.3.]Dept. of B. Voc. Food processing and Quality Management, A. A. College, Manchar. Pune (MH)

Abstract:

In this study, development of porridge using supplementary cereal that was a green gram and amaranth leaves powder which was going to enrichment the porridge and make the different other than porridge and added cereals or grains makes enrich to this porridge. In this porridge added ingredients which are cereals includes wheat, rice, sorghum and Germinated green gram and amaranth leaves powder. This multigrain porridge had a several benefits like high in nutrients and fibers. This study shows that, the sweet porridge is more acceptable on sensory basis evaluation. This porridge was also helps to reduce the malnutrition as well as prevent from other diseases. The main objective behind this research study to find out the nutrition rich food which easily available raw materials.

Keywords: grain-based snack, multigrain, nutrients-fiber rich, germinated grains

Introduction:

In India, most of traditional foods are consumed as breakfast. Wheat Porridge is a major breakfast cereal in north India as well as other parts of country it is prepared by cooking grinding of wheat in milk or water, with addition sugar or salt. It is also eating as a savory dish after cooking with water, vegetables and spices also. Its health benefits have made it a popular food worldwide.

Porridge is traditionally a breakfast i.e., simple made by cooking grains or cereals with water or milk. Different spices fruits vegetables and sweeteners such as honey can be added according to taste. Porridge can also be made using different grains including buck wheat, quinoa, brown rice and amaranth .It is food commonly eaten made by boiling ground, crushed or chopped starchy plants in water or milk. Porridge is most popular staple food which is eaten in all over developed countries, especially African countries. Porridge is a food which is made with a cereal usually oats, wheat and other grains. Sometimes oats are boiled in water

as well as milk. It is usually serving hot or most times people adds sugar or syrup to their porridge.

Cooking of porridge in large metal kettles over hot coals traditionally. Porridge was often serves as food for prisoners in prisons. T his is why in English there is a slang expression "doing porridge" which means "being in prison". Porridge is also served to those people who are ill because it is used for nourishing and easy to eat purpose. Porridge contain relatively low calories one cup of cooked porridge has just 159 calorie also you get 27 gm of total carbohydrate, 6gm of protein along with the 3gm of fat. The biggest health benefit of porridge is its fiber content. Fiber is important for making your meal more satisfying without adding calories which flush cholesterol from body. Porridge is fortified with nutrients which has significant amount of added calcium and phosphorus which benefits bone health. Porridge has also comes fortified with iron, minerals that supports your metabolism nourishes your red blood cell.

You will get generous amount of B complex vitamin which play role in produced energy. Porridge is adoptable for your diet because it absorbs the flavor of other ingredient you cooked it in sweet or salty flavoring and also create a new combination. The multigrain porridge includes different kind of grains like whole wheat, whole corn, oats, brown rice and quinoa it has several benefits like it is high in nutrients and fibers, it also lowers risk of stroke. It helpful for reduce the risk of obesity and lower risk of type diabetes. Multigrain porridge support for healthy digestion. The corn porridge called as polenta contains both protein and fibers and helps to person feel full. The polenta is gluten free rich in complex carbohydrate and vitamin A. It is source of carotenoids contents essential minerals. Polenta is low in fat as well as in calorie.

Materials and Methods:

Sorghum, Wheat, Green gram: This all cereals and pulses were purchased from local market.

Others Ingredients - other ingredients like Jaggery, fresh milk powder, amaranth was purchased vegetables from Local Market.

- **Preparation of amaranth leaves powder :**

Selection of amaranth leaves

↓

Sorting

↓

Cleaning

↓

Blanching for 2 min.

↓

Drying (3 hours at 56 ^{0}c)

↓

Grinding

↓

Screening

↓

Packaging

Germination process:

Green gram

↓

Cleaning, sorting, washing

↓

Soaking in water (12 hrs.)

↓

Tying in a muslin cloth for sprouting

↓

Germination

Porridge preparation:

Raw material (sorghum, Rice and wheat)

↓

Cleaning, sorting

↓

Grinding

↓

Flour screening /sifting

↓

Ready to use flour

Germinated flour (Green gram)

↓

Flour screening/ sifting

↓

Addition of milk powder

↓

Mixing

↓

Addition of jaggery and salt

↓

Packaging and storage

Fig: Final Product

Formulation of final product:

- **Optimization for control sample :**

Treatment	Sorghum flour (gm)	Wheat flour (gm)	Rice flour (gm)	Jaggery powder (gm)	Milk powder (gm)
T1	12	28	30	15	15
T2	13	27	25	15	20
T3	14	26	28	17	15
T4	**15**	**25**	**25**	**15**	**20**
T5	16	24	24	18	18

Fig 1: control sample

- **Variation in germinated Green Gram powder :**

Sr.No.	Treatment	S. F. (gm)	W. F. (gm)	R. F. (gm)	Jaggery (gm)	G.G (gm)	M. P. (gm)	A. L. (gm)
1	T1	16	20	20	15	10	15	4
2	T2	16	20	20	15	9	16	4
3	T3	16	20	20	15	**8**	17	4
4	T4	16	20	20	15	7	18	4
5	T5	16	20	20	15	6	19	4
6	T6	16	20	20	15	5	20	4
7	T7	16	20	20	15	4	21	4

Fig 2: Variation in germinated Green Gram powder

- **Variation in milk powder :**

Sr. No.	Treatment	S. F. (gm)	W. F. (gm)	R. F. (gm)	Jaggery (gm)	G.G (gm)	M. P. (gm)	A. L. (gm)
1	T1	16	20	20	15	10	**15**	4
2	T2	16	20	20	15	10	14	5
3	T3	16	20	20	15	10	13	6
4	T4	16	20	20	15	10	12	7
5	T5	16	20	20	15	10	11	8
6	T6	16	20	20	15	10	10	9
7	T7	16	20	20	15	10	9	10

Fig 3: variation in germinated milk powder

- **Variation in amaranth leaves powder :**

Sr. No.	Treatment	S. F. (gm)	W. F. (gm)	R. F. (gm)	Jaggery (gm)	G.G (gm)	M. P. (gm)	A. L. (gm)
1	T1	16	20	20	15	10	15	7
2	T2	16	20	20	15	11	15	**6**
3	T3	16	20	20	15	12	15	5
4	T4	16	20	20	15	13	15	4
5	T5	16	20	20	15	14	15	3
6	T6	16	20	20	15	15	15	2
7	T7	16	20	20	15	16	15	1

Fig 4: variation in amaranth leaves powder

- **Standardization of final product :**

Sr. No.	Treatment	S. F. (gm)	W. F. (gm)	R. F. (gm)	Jaggery (gm)	G.G (gm))	M. P. (gm)	A. L. (gm)
1	T1	16	20	20	15	10	15	4
2	T2	16	20	20	15	9	15	5
3	**T3**	**16**	**20**	**20**	**15**	**8**	**15**	**6**
4	T4	16	20	20	15	7	15	7
5	T5	16	20	20	15	6	15	8
6	T6	16	20	20	15	5	15	9
7	T7	16	20	20	15	4	15	10

Fig 5: standardization of final product

- **Physico-chemical analysis**

Parameter (per 100 gm) / Ingredients	Carbohydrate	Protein	Fat	Moisture (%)	Crude Fibre
Sorghum flour	65 gm	8.6gm	2.8gm	26	6gm
Wheat flour	67.50gm	11.80gm	1.20gm	12	9.8gm
Rice flour	23.10gm	2.98gm	-	10.50	0.2gm
Jaggery	92.76gm	0.07gm	-	46	-
Green gram	36.02gm	11.9gm	0.6gm	12	13.7gm
Milk powder	36.00gm	24.7gm	24gm	4.3	-
Amaranth leaves	61.92gm	11.43gm	6.9gm	5.49	6.2gm

Fig 6: physico-chemical analysis

Mineral analysis (mg/100gm)

Minerals / Ingredients	Calcium	Sodium	Iron	Magnesium	Potassium	Manganese	Zinc
Amaranth Flour	2597.00	12.60	14.80	1149.00	5893.00	21.96	6.10
Germinated Green gram	11450	4.35	82000	69.84	73.52	43000	22891

Fig 7: mineral analysis

Conclusion:

On the basis of present investigation, it concluded that porridge is made from sorghum flour, wheat flour, green gram powder, milk powder and jaggery powder in adequate amount with the addition of amaranth leaves powder in a good sensory attributes. Selected control sample used for addition of both ingredients i.e. amaranth leaves and green gram powder has increase the nutritional and functional value of this product. Both the powder which prevent from anemic, reduce bad cholesterol, rich in antioxidant, storehouse of nutrients and also rich source of proteins and vitamins. Folate in green gram help in healthy pregnancy and also helps for reduce high blood pressure. Nutraceutical value of porridge was increased since both powders contain flavonoids, phenolic acid, β- carotene, phenolics and antioxidants.

Reference:

1. .AOAC (2005). Determination of Moisture, Ash, Protein and Fat. Official Methods of Analysis. 18th ed. Association of Official Analytical Chemists, Washington, DC.
2. Ajifolokun, O. M., Basson, A. K., Osunsanmi, F. O., & Zharare, G. E. (2019). Nutritional Composition and Organoleptic Properties of Composite Maize Porridge. J Food Process Technol, 10(798),
3. Dhital, a. (2021). preparation of porridge from germinated multigrain and its nutritional evaluation (doctoral dissertation, department of nutrition and dietetics central campus of technology institute of science and technology tribhuvan university, nepal 2021).
4. Fana Haile, S. A., &Fisseha, A. (2015). Effects of pre-treatments and drying methods on chemical composition, microbial and sensory quality of orange-fleshed sweet potato flour and porridge. American Journal of Food Science and Technology, 3(3), 82-88.
5. Gantwerker, S., & Leong, S. (1984). U.S. Patent No. 4,438,150. Washington, DC: U.S. Patent and Trademark Office.

6. Gebretsadikan, T. M., Bultosa, G., Forsido, S. F., &Astatkie, T. (2015). Nutritional quality and acceptability of sweet potato–soybean–moringa composite porridge. Nutrition & Food Science.
7. Helland, M. H., Wicklund, T., &Narvhus, J. A. (2002). Effect of germination time on alpha-amylase production and viscosity of maize porridge. Food Research International, 35(2-3), 315-321.
8. Kabeir, B. M., Abd- Aziz, S., Muhammad, K., Shuhaimi, M., & Yazid, A. M. (2005). Growth of Bifidobacterium longum BB536 in medida (fermented cereal porridge) and their survival during refrigerated storage. Letters in applied microbiology, 41(2), 125-131.
9. Lee, I., Shi, L., Webb, D. L., Hellström, P. M., Risérus, U., &Landberg, R. (2016). Effects of whole-grain rye porridge with added inulin and wheat gluten on appetite, gut fermentation and postprandial glucose metabolism: a randomised, cross-over, breakfast study. British Journal of Nutrition, 116(12), 2139-2149.
10. Mounika, J., Vellanki, B., Neelima, T., Guggilla, M., & Maloo, S. Study on the Drying Characteristics of Green Gram, Cowpea and Soybean. International Journal of Advanced Engineering, Management and Science, 3(9), 239918.
11. Nahemiah, D., Nkama, I., &Badau, M. H. (2016). Application of response surface methodology (RSM) for the production and optimization of extruded instant porridge from broken rice fractions blended with cowpea. Sciences, 5(2), 105-116.
12. Nefale, F. E., &Mashau, M. E. (2018). Effect of germination period on the physicochemical, functional and sensory properties of finger millet flour and porridge. Asian Journal of Applied Sciences, 6(5).
13. Nicole, M., Fei, H. Y., & Claver, I. P. (2010). Characterization of ready-to-eat composite porridge flours made by soy-maize-sorghum-wheat extrusion cooking process. Pakistan Journal of Nutrition, 9(2), 171-178.
14. Pavadhgul, P., Bumrungpert, A., Harjani, Y., & Kurilich, A. (2019). Oat porridge consumption alleviates markers of inflammation and oxidative stress in hypercholesterolemic adults. Asia Pacific journal of clinical nutrition, 28(2), 260-265.
15. Peiretti, P. G. (2018). Amaranth in animal nutrition: A review. Livestock Research for Rural Development, 30(5), 1-20.
16. Singh, A., &Punia, D. (2019). Development and quality evaluation of optimized traditional food porridge formulation based on processed amaranth grain. IJCS, 7(5),43-45.
17. Shakoor, S., Kanwal, A., Abbas, N., Mirza, M. A., &Arif, S. (2014). Effect of natural dietary fibers (wheat porridge) on hyperlipidemia rats. J Global Innov Agri Soc Sci, 2, 39-44.

Paper 48

Photocatalytic degradation of Xylenol Orange dye over hydrothermally synthesized Zinc Oxide

Yogeshwar Digambar Kaldante[1,3,*], Manohar Ganpat Chaskar[1,2,*]

[1.] *Department of Chemistry, PDEA's Baburaoji Gholap College, Sangvi, Pune, Maharashtra*

[2.] *Department of Chemistry, PDEA's Prof. Ramkrishna More College, Akurdi, Maharashtra*

[3.] *Department of Chemistry, PDEA's Annasaheb Waghire College, Otur, Pune, Maharashtra*

Abstract

Present work discusses the hydrothermal synthesis of ZnO, its characterization and application for the photocatalytic degradation (PCD) of Xylenol Orange dye. Hydrothermal synthesis of ZnO involves formation of Zinc hydroxide precursor. The process of conversion of this Zinc hydroxide to ZnO was examined by TGA-DTG analysis and FT-IR Spectroscopy, XRD peak data indicated hexagonal wurtzite crystallite structures of ZnO. FESEM image of ZnO confirmed nanocrystalline hexagonal rod-like morphologies of ZnO particles. EDX spectrum confirmed the elemental purity of ZnO. The UV-DRS study was used to deliberate the optical band gap of ZnO. Optical properties of ZnO were also studied with PL spectroscopy. Considering Xylenol Orange as a model organic dye the PCD experiments was carried out to deliberate the activity of ZnO. The PCD efficiency of ZnO was estimated by colorimetric absorbance monitoring. The catalytic activity was studied with reference to the condition of photocatalyst loading capacity, pH of dye solution, dye concentration, irradiation time, etc.

Keywords: *Zinc Oxide; Xylenol Orange; Hydrothermal method; PCD efficiency;*

1. Introduction

The electrical, mechanical, optical and chemical properties of the nanomaterial semiconductors can be tuned by varying their particle dimensions which makes them valuable for various applications **[1]**. Among semiconductor materials metal oxides are proven to be the promising materials towards the vary wide range of applications such as sensing **[2]**, catalysis **[3]**, energy storage, conversion optics, electronic devices **[4, 5]**, memory arrays, biomedical application **[6, 7]** and acoustic wave devices **[8]**. Due to unique physico-chemical properties of the zinc oxide

it is most widely investigated semiconductor metal oxide. ZnO is a direct wide band gap (3.37 eV) semiconductor material possessing high exciton binding energy (60 meV) **[1, 9]**. ZnO shows strong optoelectronic, piezoelectric and pyroelectric properties **[9, 10]**. Also due to the environmentally friendly nature, biocompatibility, and thermal stability of the ZnO nanomaterials, these are the most promising contender for optoelectronic and electronic applications including sensors, actuators, light emitting diodes (LEDs), solar cells, field-emission devices, ultra-violet laser diodes, photocatalysts, as well as spintronic and piezoelectric devices **[10]**. ZnO nanostructures can be synthesized by using various synthetic methods such as mechanochemical **[11]**, solution combustion **[12]**, chemical precipitation **[13, 14]**, sol-gel method **[15]**, hydrothermal synthesis **[16, 17]**, etc. Among these methods hydrothermal method is one of the auspicious alternative synthetic method due to low process temperature and very easy to control the particle size **[1]**. In addition to this hydrothermal method is associated with several advantages such as low cost, large area uniform production, use of simple equipment, less hazardous, environmental friendliness, catalyst-free growth **[1]**. The size and morphology of the particle can be controlled by tuning concentration of precursors, reaction temperature and time in the hydrothermal process hence it is well recognized method to obtain the nanomaterials with classified morphologies and particle sizes. Advanced Oxidation Processes (AOPs) proven to be the efficient tool for the environmental technology. Among AOPs heterogeneous photocatalysis is one of the well-established and best alternatives for the replacement of conventional methods of water treatment **[18]**. Among AOPs the photocatalysis is most efficient and economical method that is giving the total mineralization of organic contaminants to CO_2, H_2O and inorganic salts **[19]**. Among the different metal oxide semiconductor photocatalysts, ZnO is most vastly studied photocatalytic degradation material for environmental pollutants, because of its low cost, nontoxic nature and high photochemical reactivity **[20]**.

In the present work, ZnO was synthesized by the hydrothermal method and its photocatalytic activity was tested by means of degradation of xylenol orange dye. The photocatalytic activity was studied with reference to the condition of pH of dye solution, photocatalyst loading capacity, dye concentration, irradiation time, etc.

2. Experimental

2.1 Materials

Zinc acetate dihydrate (assay 99.5%), Xylenol Orange (assay 99.0%), Liquor ammonia and supplementary essential chemicals used as-received during this work were AR grade reagents obtained from S.D. Fine Chemicals, India. All the related experimental solutions were prepared in distilled water. Wherever necessary, pH of the relevant solutions was agreed to desired values with NaOH (0.1N) and HCl (0.1N).

2.2. Synthesis of photocatalyst

Zinc Oxide (ZnO) nanoparticles were synthesized as follows: To the 120 ml solution of 0.5M zinc acetate dihydrate, 8 ml liquor ammonia was added in a dropwise manner under vigorous magnetic stirring for the 2 hours. The pH of the reaction mixture was ensured to be fairly alkaline. The white suspension thus obtained was further magnetically stirred for another 1 hour to ensure homogeneous phase. The small quantity of white precipitate (zinc hydroxide) from this solution was isolated, dried and preserved for the thermal analysis. The suspension was then transferred to the teflon-lined container, which is placed in a stainless steel autoclave / hydrothermal reactor. Autoclave was properly sealed and maintained at 150 ^{0}C for 4 hours under autogenous pressure. It was then permitted to cool naturally to room temperature. After completion of reaction the resultant white residue was filtered and washed with water followed by ethanol and finally dried at 100 ^{0}C.

2.3. Equipments

The conversion temperature of zinc hydroxide to ZnO was studied by thermogravimetric analysis machine (Shimadzu, TG - DTG - 60H) and FT-IR (PerkinElmer UATR Spectra Two) spectrometer. The X-ray diffraction (XRD) patterns of pure ZnO earned with X-ray Diffractometer (Rikagu Miniflex-600) via Cu Kα radiation ($\lambda\alpha$ = 1.5418Å) and the average crystallite size (D) was estimated from the Debye-Scherer equation: $D = 0.90\lambda / \beta\cos\theta$ where, λ is the wavelength (Cu Kα), β is the full width at the half maximum (FWHM) of the most intense peak (101) in the XRD pattern of samples and θ is the diffraction angle **[21]**. The morphological description of ZnO was accomplished by using FE-SEM (JEOL JSM-6360A). The elemental purity of ZnO was studied with energy dispersive X-ray (EDX) spectra. The optical band gap of ZnO was estimated from

UV-Visible spectra and Tauc plots gained with UV-Visible Spectrophotometer (PerkinElmer Lambda 365). All the PCD reactions were carried out at room temperature in solar light in batch reactor. Colorimetric absorbance measurement with digital colorimeter (EQUIP-TRONICS EQ-353) is chosen to decide the degradation efficiency. The preliminary pH of suspension was in tune with the help of pH meter (LABTRONICS LT-11). Lux meter (HTC LX-100) is used for consistent measurement of the light intensity.

2.4. Photocatalytic degradation experiments

The photocatalytic degradation efficiency of the hydrothermally synthesized ZnO was elaborated by means of degradation of xylenol orange dye. All the experimental dye solutions were prepared using distilled water with diverse initial concentrations. All experiments are executed in a batch photoreactor with glass cool trap and magnetic stirrer. Xylenol Orange (100 mL) dye solution having known original concentration at apposite pH and at room temperature was taken with known extent of photocatalyst in a cylindrical photoreactor having 5 cm inner diameter. The uniform suspension of the reaction mixture was got by means of ultrasonic agitation for 5 minutes. Container was then placed on magnetic stirrer kept under irradiation of solar light. At specified time intervals supernatant solution was collected and centrifuged to settle down photocatalyst particles. Then absorbance of centrifuged supernant solution was recorded at predetermined λ_{max} value of Xylenol Orange dye solution using digital colorimeter. The PCD efficiency was estimated from absorbance measurement as percent (%) Degradation: $\%D = 100[A_0 - A_t] / [A_0]$ where %D – Percent Degradation, A_0-Initial absorbance, A_t -Absorbance at time *t*.

3. Result and discussion

3.1. Characterization of ZnO

3.1.1. Thermal gravimetric analysis

Figure 1 shows the TGA-DTG plots for zinc hydroxide synthesized at the initial stage of hydrothermal synthesis of ZnO. As per DTG curve, the two endothermal steps are associated within the temperature range from 110 ^{0}C to 215 ^{0}C during the conversion of zinc hydroxide to ZnO. Both these stages collectively associated with the loss of water from zinc hydroxide and are corresponding to the weight losses 13.18% and 9.08% respectively.

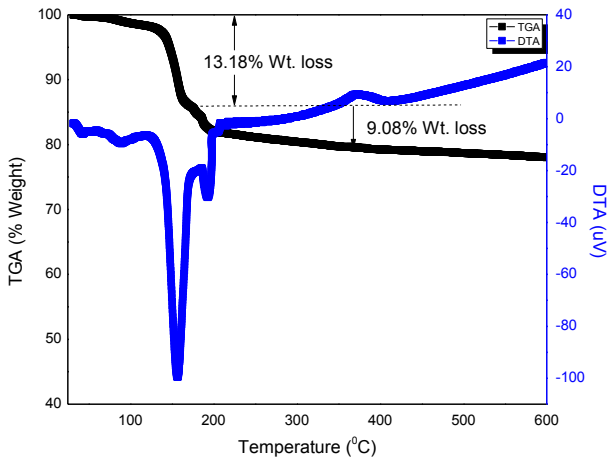

Figure 1: TGA-DTG analysis of zinc hydroxide

3.1.2. FT-IR Spectroscopic Study

Figure 2 is for FT-IR spectra of hydrothermal synthesis of ZnO. The foremost frequency changes and bands assignment in the region 4000–400cm^{-1} within the FT-IR spectra during the makeover of zinc hydroxide to zinc oxide are mentioned here. The FT-IR spectra of $Zn(OH)_2$ consists bands equivalent to various symmetric and asymmetric stretching and bending vibrations recognized at 450, 8368, 1390, 1515, and 1550 cm^{-1}. Calcination of sample at 400 ^{0}C results in diminishing of the all bands except than at 450cm^{-1} in confirmation with the formation of spherical shape ZnO and same also suggested by XRD and EDS study.

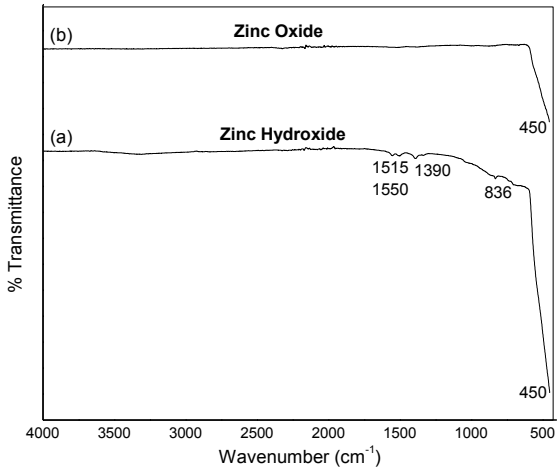

Figure 2: FT-IR spectra of hydrothermal synthesis of ZnO

3.1.3. X-Ray Diffraction (XRD) Study

The XRD intensity data collected for hydrothermally synthesized ZnO over a 2θ range of 20^0-80^0 with Cu Kα radiation (λ=1.5418 Å) showing a series of peaks placed at 2θ = 31.80°, 34.46°, 36.30°, 47.60°, 56.64°, 62.90°, 66.40°, 67.98°, 69.12°, 72.60°, 77.00° fitting to (100), (002), (101), (102), (110), (103), (200), (112), (201), (004) and (202) crystal planes respectively (**Figure 3**). This data was found to be in accordance with JCPDS card 36-1451 for the standard wurtzite structure of pure ZnO **[22]**. The estimated average crystallite size of ZnO as per Debye Scherer's formula **[21]** was 30.73 nm with FWHM = 0.2574^0 for highest intensity peak corresponding to (101) plane.

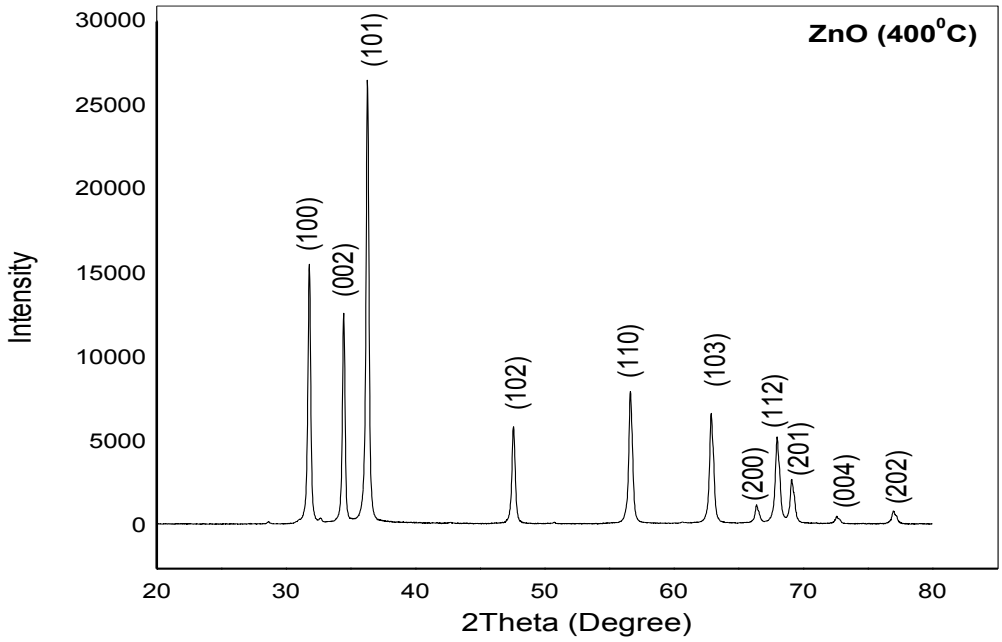

Figure 3: XRD pattern of ZnO

3.1.4. FE-SEM Study

Figure 4 denotes FE-SEM photographic images of hydrothermally synthesized ZnO sample. The FE-SEM photograph denotes homogeneous phase with hard particles having hexagonal rod-like morphologies. Sample is found with nearly uniform particle size distribution.

Figure 4: FE-SEM image of ZnO

3.1.5. EDX analysis

Figure 5 shows EDX spectrum of ZnO sample, which consist of peaks corresponding to only Zn and O elements as a reflection of elemental purity of the ZnO sample.

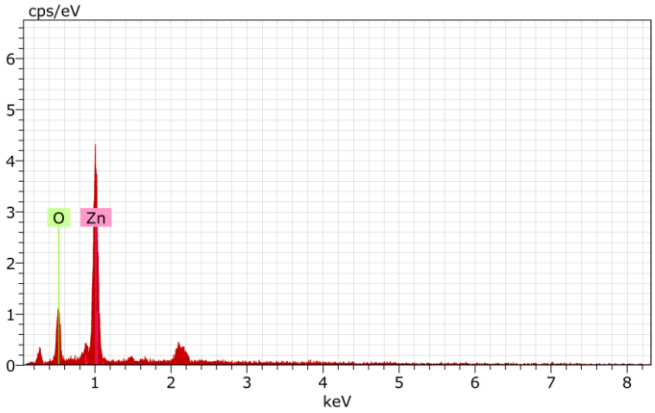

Figure 5: EDX spectrum of ZnO

3.1.6. UV-Visible Spectra

Figure 6 (a) indicate UV-visible spectrum and **Figure 6 (b)** indicate Tauc plot of ZnO sample. UV- Visible spectra has optical extinction band situated in the wavelength range 370nm to 420nm with cutoff wavelength 403.81nm related to the bulk ZnO absorption **[23]**. From Tauc plot estimated bandgap of ZnO was found to be 3.071eV.

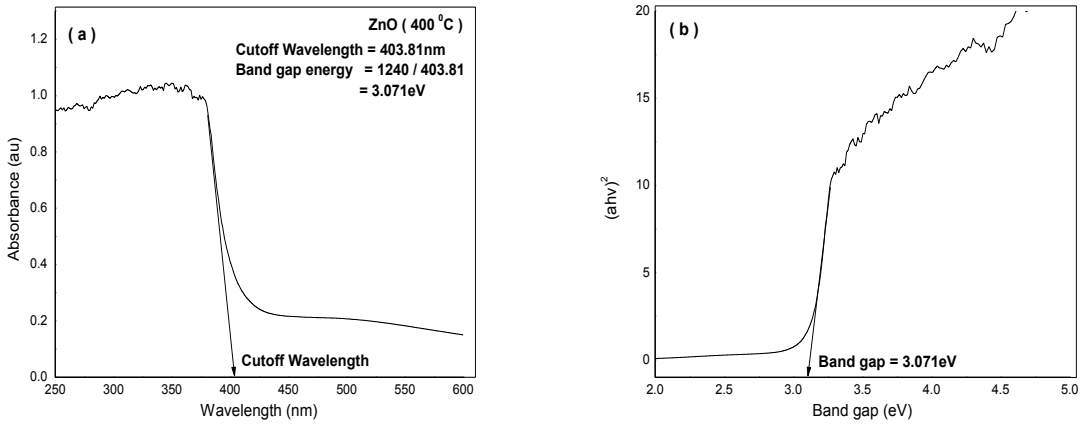

Figure 6: UV-visible spectrum **(a)** and Tauc plot **(b)** of ZnO

3.1.7. Photoluminescence (PL) Spectra

Figure 7 shows room temperature PL spectrum of ZnO synthesized by hydrothermal method recorded with excitation wavelength 320nm to study defect in ZnO as well as further investigation of its optical properties. As sign of good crystallanity ZnO shows a less intense but noticeable UV (Near Band Edge) emission peak **[24]** centered near 382nm due to excitonic recombination matching to the band edge emission of ZnO sample **[25, 26]**. ZnO has intense emission band at 500nm in PL spectrum due to green emission because of radiative recombination of photogenerated holes with electrons occupying oxygen vacancies **[26]**.

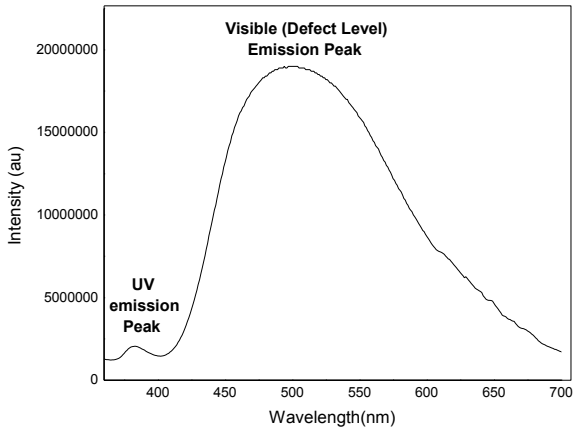

Figure 7: Room Temperature PL spectrum of ZnO

3.2. Photocatalytic Activity of ZnO

Photocatalytic activity of hydrothermally synthesized ZnO was examined with distinctive reference to the operative parameters such as pH of dye solution, photocatalyst loading capacity, dye initial concentration, irradiation time, etc.

3.2.1 Effect of the initial pH of Xylenol Orange dye solution

The PCD of 100 ppm of Xylenol Orange dye over hydrothermally synthesized ZnO was studied at different pH from 6 to 11 with ZnO loading of 125mg / 100ml of dye solution and with 6 hours of sunlight irradiation (**Figure 8**). The measurements of pH of the suspensions only consider before irradiation and not controlled during the course of reaction. As per fine recognized fact, slight (<1%) dissolution of the ZnO in acidic medium reduces its PCD efficiency at pH 6 **[27]**. The extent of Xylenol Orange dye PCD was found to increase with the increase in initial pH of suspensions. Excess of hydroxyl anions in alkaline medium stimulates photo-generation of the main oxidizing species (hydroxyl radicals) responsible for PCD **[28]**. Hence, PCD efficiency of ZnO was observed to be more at alkaline pH (9-11) and at pH 11 the PCD efficiency was highest.

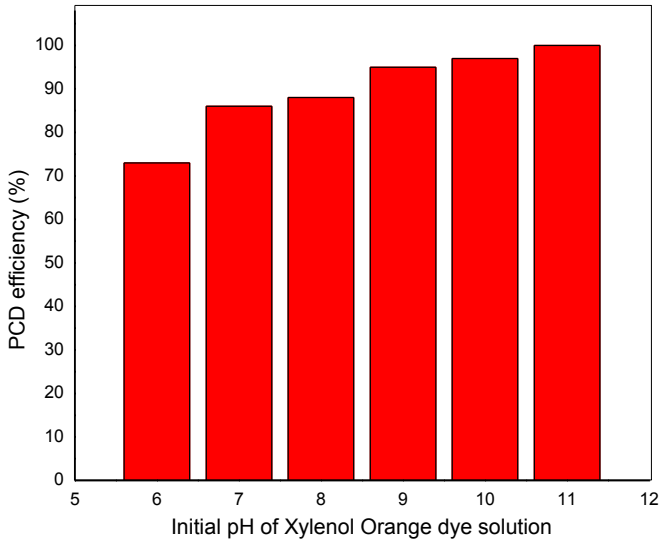

Figure 8: Effect of the initial pH of Xylenol Orange dye solution

3.2.2 Effect of the loading of ZnO photocatalyst

The PCD of 100 ppm of Xylenol Orange over hydrothermally synthesized ZnO was studied at different loading amounts of ZnO from 50mg/100ml to 200mg/100ml of dye solution at pH=11 and with 6 hours of sunlight irradiation (**Figure 9**). It was observed that, the PCD efficiency was slowly increased up to ZnO loading amount of 125mg/100ml of dye solution and acquire constancy beyond this limit. The number of active sites on the photocatalyst surface increased with its amount, which in sequence increased the number of hydroxyl, and superoxide radicals **[22]**. Hence, PCD efficiency increases with ZnO loading upto 125mg/100ml of dye solution. Beyond this limit, the PCD efficiency acquire stability this is may be due to the availability of more number of active species for the degradation of same number of dye molecules. Hence, 125mg ZnO /100ml of dye solution is adequate for the complete degradation of Xylenol Orange within 6 hours of irradiation.

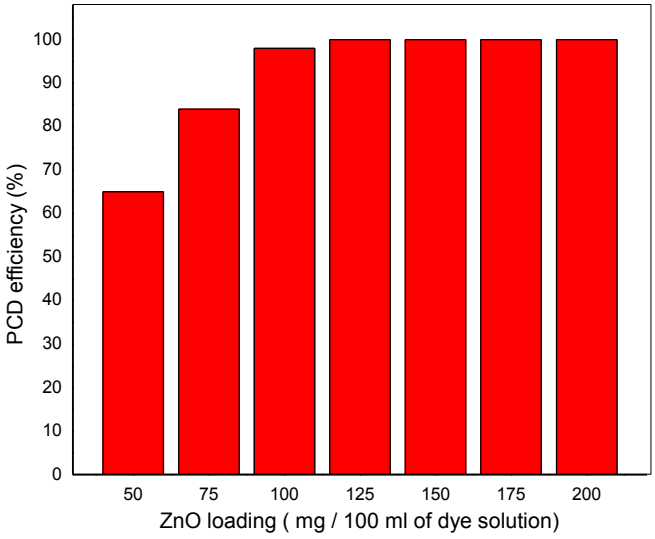

Figure 9: Effect of the loading of ZnO photocatalyst

3.2.3 Effect of the initial concentration of Xylenol Orange dye solution

The degradation efficiency of Xylenol Orange over hydrothermally synthesized ZnO at varied initial concentrations in the range 50- 200ppm was inspected as a function of sunlight irradiation time at the pH 11 of the suspension. The PCD efficiency is measured in terms of increase in % degradation of Xylenol Orange and results are shown in **Figure 10**. The each of 50ppm and 100ppm of Xylenol Orange was totally mineralized over 125mg ZnO/100ml of the dye solution. As per the prediction, increase in concentration of dye solutions decreases the PCD efficiency. This is due to the formation of deep colored and turbid solution which generates obstacle in the path of light photons and hence reduces their absorption by the photocatalyst surface which results in the reduction of active radical species production responsible for the PCD **[29]**.

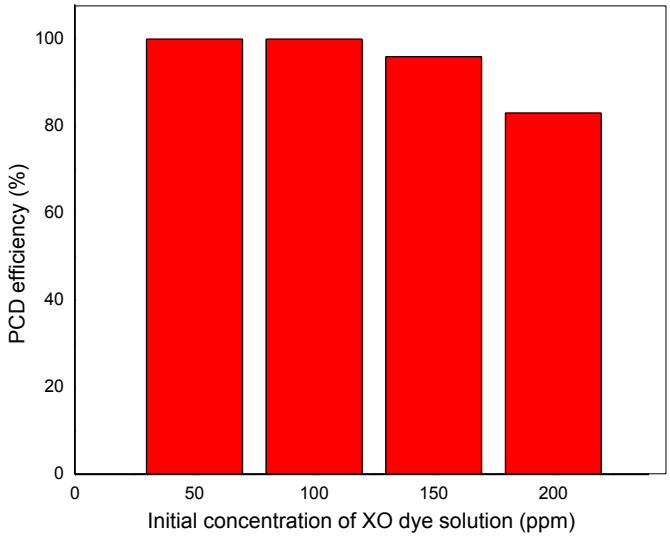

Figure 10: Effect of the initial concentration of Xylenol Orange dye solution

3.2.4 Effect of irradiation time

The PCD efficiency of ZnO in sunlight gradually increases with increase in irradiation time (**Figure 11**). 100ml of 100ppm Xylenol Orange dye solution was completely mineralized over 125mg ZnO at the pH 11 upon 6 hours of sunlight irradiation. Irradiation time linearly affects the PCD efficiency.

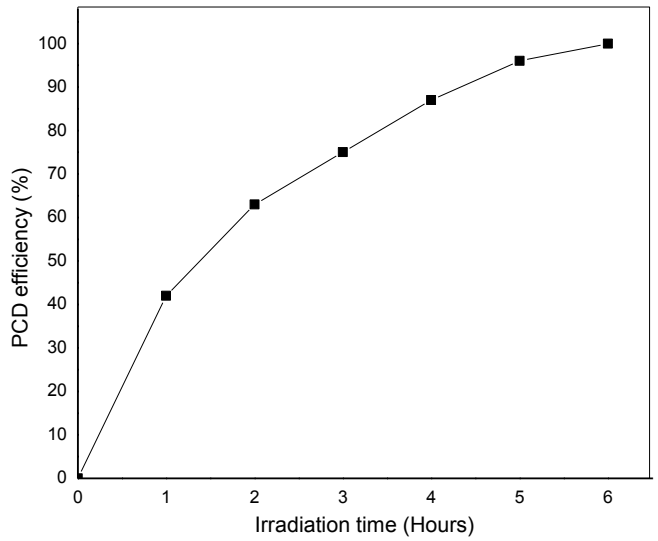

Figure 11: Effect of irradiation time

The **Figure 12** shows the UV-Visible spectra presenting PCD of Xylenol Orange dye with irradiation time. As per **Figure 12**, the absorbance of Xylenol Orange dye solution declines with increase in irradiation time and nearly becomes zero within 6 hours of irradiation.

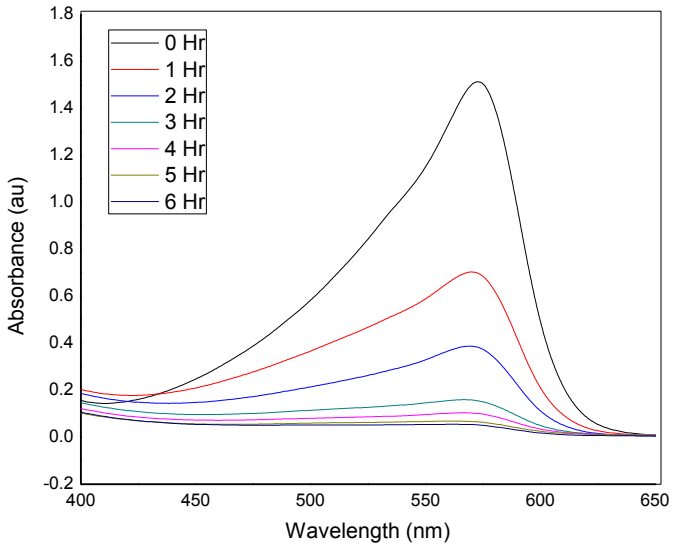

Figure 12: UV-Visible spectra showing PCD of Xylenol Orange dye

4. Conclusions

In the present investigation, we have reported the hydrothermal synthesis of ZnO photocatalysts. This ZnO photocatalyst was obtained via zinc hydroxide precursors. The formation of ZnO was confirmed by TGA- DTG analysis, FT-IR Spectroscopy, XRD technique, FE-SEM technique, EDX technique, UV-Visible and PL spectroscopies. XRD pattern of ZnO matches with hexagonal wurtzite structure. FE-SEM photograph indicates the formation of denser hexagonal rod-like particles of ZnO. EDX spectrum explains the elemental purity of ZnO sample. UV-Visible and PL spectroscopies successfully explain the optical properties of ZnO nanoparticles. The 100ml each of 50ppm and 100ppm of Xylenol Orange dye solutions at pH 11 were completely mineralized over 125mg ZnO within 4 and 6 hours of sunlight irradiation respectively. The effect of various operative factors on PCD of Xylenol Orange dye was successfully inspected.

5. Acknowledgements

Authors are exclusively grateful to PDEA's Baburaoji Gholap College, Sangvi and Annasaheb Waghire College, Otur for providing their continuous and valuable support, in terms of amenities like laboratories for all experimental work, instrumental facilities for the characterization of materials and libraries for the literature review.

6. References

[1] Madathil, Aneesh N. Pacheri, K. A. Vanaja, and M. K. Jayaraj. "Synthesis of ZnO nanoparticles by hydrothermal method." In *Nanophotonic materials IV*, vol. 6639, p. 66390J. International Society for Optics and Photonics, 2007.

[2] Sonker, Rakesh Kumar, Anjali Sharma, Md Shahabuddin, Monika Tomar, and Vinay Gupta. "Low temperature sensing of NO2 gas using SnO2-ZnO nanocomposite sensor." *Adv. Mat. Lett* 4 (2013): 196-201.

[3] Irfan, Muhammad Faisal, Ahsanulhaq Qurashi, and Mir Wakas Alam. "Metal oxide nanostructures and nanocomposites for selective catalytic reduction of NOx: a review." *The Arabian Journal for Science and Engineering* 35 (2010): 79-92.

[4] Purica, Munizer, Elena Budianu, and Emil Rusu. "ZnO thin films on semiconductor substrate for large area photodetector applications." *Thin Solid Films* 383, no. 1-2 (2001): 284-286.

[5] Aoki, Toru, Yoshinori Hatanaka, and David C. Look. "ZnO diode fabricated by excimer-laser doping." *Applied Physics Letters* 76, no. 22 (2000): 3257-3258.

[6] Kunjara Na Ayudhya, Sirachaya, Parawee Tonto, Okorn Mekasuwandumrong, Varong Pavarajarn, and Piyasan Praserthdam. "Solvothermal synthesis of ZnO with various aspect ratios using organic solvents." *Crystal growth & design* 6, no. 11 (2006): 2446-2450.

[7] Wu, Changle, Xueliang Qiao, Jianguo Chen, Hongshui Wang, Fatang Tan, and Shitao Li. "A novel chemical route to prepare ZnO nanoparticles." *Materials Letters* 60, no. 15 (2006): 1828-1832.

[8] Gorla, C. R., N. W. Emanetoglu, S. Liang, W. E. Mayo, Y. Lu, M. Wraback, and H. Shen. "Structural, optical, and surface acoustic wave properties of epitaxial ZnO films grown on (0112) sapphire by metalorganic chemical vapor deposition." *Journal of Applied Physics* 85, no. 5 (1999): 2595-2602.

[9] Baruah, Sunandan, and Joydeep Dutta. "Hydrothermal growth of ZnO nanostructures." *Science and technology of advanced materials* 10 (2009) 013001 (18pp).

[10] Samadi, Morasae, Mohammad Zirak, Amene Naseri, Elham Khorashadizade, and Alireza Z. Moshfegh. "Recent progress on doped ZnO nanostructures for visible-light photocatalysis." *Thin Solid Films* 605 (2016): 2-19.

[11] Shen, Liming, Ningzhong Bao, Kazumichi Yanagisawa, Kazunari Domen, Arunava Gupta, and Craig A. Grimes. "Direct synthesis of ZnO nanoparticles by a solution-free mechanochemical reaction." *Nanotechnology* 17, no. 20 (2006): 5117.

[12] Ali, Mohammad Amdad, Mahmudur Rahman Idris, and Md Emran Quayum. "Fabrication of ZnO nanoparticles by solution-combustion method for the photocatalytic degradation of organic dye." *Journal of Nanostructure in Chemistry* 3, no. 1 (2013): 1-6.

[13] Zhong, Qiping, and Egon Matijević. "Preparation of uniform zinc oxide colloids by controlled double-jet precipitation." *Journal of Materials Chemistry* 6, no. 3 (1996): 443-447.

[14] Wang, Lingna, and Mamoun Muhammed. "Synthesis of zinc oxide nanoparticles with controlled morphology." *Journal of Materials Chemistry* 9, no. 11 (1999): 2871-2878.

[15] Bahnemann, Detlef W., Claudius Kormann, and Michael R. Hoffmann. "Preparation and characterization of quantum size zinc oxide: a detailed spectroscopic study." *Journal of physical chemistry* 91, no. 14 (1987): 3789-3798.

[16] Zhang, Hui, Deren Yang, Xiangyang Ma, Yujie Ji, Jin Xu, and Duanlin Que. "Synthesis of flower-like ZnO nanostructures by an organic-free hydrothermal process." *Nanotechnology* 15, no. 5 (2004): 622.

[17] Li, Wen-Jun, Er-Wei Shi, Yan-Qing Zheng, and Zhi-Wen Yin. "Hydrothermal preparation of nanometer ZnO powders." *Journal of materials science letters* 20, no. 15 (2001): 1381-1383.

[18] Rashed, M. N., and A. A. El-Amin. "Photocatalytic degradation of methyl orange in aqueous TiO2 under different solar irradiation sources." *International Journal of Physical Sciences* 2, no. 3 (2007): 73-81.

[19] Rajeshwar, K., M. E. Osugi, W. Chanmanee, C. R. Chenthamarakshan, Maria Valnice Boldrin Zanoni, P. Kajitvichyanukul, and R. Krishnan-Ayer. "Heterogeneous photocatalytic treatment of organic dyes in air and aqueous media." *Journal of photochemistry and photobiology C: photochemistry reviews* 9, no. 4 (2008): 171-192.

[20] Elamin, Nazar, and Ammar Elsanousi. "Synthesis of ZnO nanostructures and their photocatalytic activity." *Journal of Applied and Industrial Sciences* 1, no. 1 (2013): 32-35.

[21] Wu, Ling, C. Yu Jimmy, and Xianzhi Fu. "Characterization and photocatalytic mechanism of nanosized CdS coupled TiO2 nanocrystals under visible light irradiation." *Journal of Molecular Catalysis A: Chemical* 244, no. 1-2 (2006): 25-32.

[22] Pardeshi, S. K., and A. B. Patil. "Effect of morphology and crystallite size on solar photocatalytic activity of zinc oxide synthesized by solution free mechanochemical method." *Journal of Molecular Catalysis A: Chemical* 308, no. 1-2 (2009): 32-40.

[23] Pan, Anlian, Richeng Yu, Sishen Xie, Zebo Zhang, Changqing Jin, and Bingsuo Zou. "ZnO flowers made up of thin nanosheets and their optical properties." *Journal of Crystal Growth* 282, no. 1-2 (2005): 165-172.

[24] Xu, Linping, Yan-Ling Hu, Candice Pelligra, Chun-Hu Chen, Lei Jin, Hui Huang, Shanthakumar Sithambaram, Mark Aindow, Raymond Joesten, and Steven L. Suib. "ZnO with different morphologies synthesized by solvothermal methods for enhanced photocatalytic activity." *Chemistry of Materials* 21, no. 13 (2009): 2875-2885.

[25] Yu, Shi-Yong, Hong-Jie Zhang, Ze-Ping Peng, Li-Ning Sun, and Wei-Dong Shi. "Template-free fabrication of hexagonal ZnO microprism with an interior space." *Inorganic chemistry* 46, no. 19 (2007): 8019-8023.

[26] Huang, Michael H., Yiying Wu, Henning Feick, Ngan Tran, Eicke Weber, and Peidong Yang. "Catalytic growth of zinc oxide nanowires by vapor transport." *Advanced materials* 13, no. 2 (2001): 113-116.

[27] Behnajady, M. A., N. Modirshahla, and R. Hamzavi. "Kinetic study on photocatalytic degradation of CI Acid Yellow 23 by ZnO photocatalyst." *Journal of hazardous materials* 133, no. 1-3 (2006): 226-232.

[28] Muruganandham, M., and M. Swaminathan. "Solar photocatalytic degradation of a reactive azo dye in TiO2-suspension." *Solar Energy Materials and Solar Cells* 81, no. 4 (2004): 439-457.

[29] Shirsat Ramesh Natha, Manohar Ganpat Chaskar, Yogeshwar Digambar Kaldante, Yogesh B. Khollam, Tm-doped ZnO: an efficient catalyst for photodegradation of methylene blue under sunlight irradiation, Journal of Emerging Technologies and Innovative Research (JETIR) May 2019, Volume 6, Issue 5, pp. 150-162.

Paper 49

Properties of Samarium Polonide with Nacl-type Structure

Jagdeesh Pataiya[a*], Lokesh Jharbade[b], Nilesh Dhurve[c], Neetu Paliwal[d], Satish Bagde[e]

[a]Department of Physics, Dr. Bhimrao Ambedkar Govt. College, Alma,

[b]Department of Chemistry, Dr. Bhimrao Ambedkar Govt. College, Amla,

[c]Department of Physics, Govt. College, Bhimpur, Betul

[d]Department of Physics, Rabindranath Tagore University, Bhopal,

[f]Department of Library, Dr. Bhimrao Ambedkar Govt. College, Amla

---

Abstract: First-principles full-potential linearized augmented plane wave (FP-LAPW) method within density functional theory (DFT) potentials has been used to calculate lattice parameter, total energy, phase transition pressure, elastic constant and electronic properties of SmPo at ambient as well as at high pressure. The calculations were performed within the generalized gradient approximation (GGA) and local spin density approximation (LSDA) for the exchange–correlation. From our calculations we observe that SmPo is stable in NaCl – type structure under ambient pressure. For this compound, the phase transition pressure was found to be 8 GPa. All properties obtained are in good agreement with available theoretical and experimental data.

Keywords: Phase transition in solid; Band structure.

1. Introduction

The high pressure behavior of samarium and their compounds with NaCl-type structure has been a subject of extensive research in condensed matter physics [1]. These compounds received considerable interest because of their electronic, magnetic, optical and phonon properties. The compounds e.g. sulphides, selenides, tellurides of cerium, samarium, yttrium, ytterbium, europium, thulium and their alloys show non integral valence between 2 and 3, arising due to *f-d* electron hybridization at ambient pressure and temperature. Svane et al. [2] has been studied electronic properties of Sm and Eu chalcogenides using SIC-LSD approach and reported that the SIC-LSD total energy predicts a valency transition of samarium between the Sm pnictides and the

Sm chalcogenides. The continuous insulator-to-metal transition in bulk crystalline rare-earth monochalcogenide materials has been experimentally studied beginning with the pioneering diamond anvil cell work of Jayaraman et al. [3, 4]. Using the self-interaction corrected local-spin density approximation the electronic structures of Sm chalcogenides are reported [5]. With six localized *f*-electrons, the chalcogenides are semiconductors, which are the ground state of SmS, SmSe, and SmTe. Under compression the Sm chalcogenides undergo first order transitions with destabilization of the *f*-states into the intermediate valence state.

In the present study we have reported high pressure structural and electronic properties of samarium polonide (SmPo) at ambient and high pressure. We have calculated the electronic structure, band structure, structural stability and total energy of this compound using the density functional theory within generalized gradient approximation (GGA).

2. Method of Calculation

FP-LAPW method within density functional theory as implemented in the WIEN2k code [6] has been used to study the structural and electronic properties of SmPo. LSDA [7] and PBE-GGA [8] approximations have been used to determine the optimized structure of this compound. In the FP-LAPW method, the wave function, charge density and potential are expanded by spherical harmonic functions inside non-overlapping spheres surrounding the atomic sites (muffin-tin spheres) and by a plane wave basis set in the remaining space of the unit cell (interstitial region). In order to achieve the energy eigen value convergence, we expanded the basis function up to RMT * Kmax = 8 where RMT is the smallest atomic sphere radius in the unit cell and Kmax gives the magnitude of the largest K vector in the plane wave expansion. The valence wave functions inside the spheres are expanded up to lmax = 10 while the charge density is Fourier expanded up to Gmax = 12. The self-consistent calculations are considered to converge when the total energy of the system is stable.. A dense mesh of 1000 k points is used and the tetrahedral method has been employed for the Brillouin zone integration. The total energies are calculated as a function of volume and fitted to Birch equation of state [9] to obtain the ground state properties.

3. Results and Discussion

In order to calculate the ground state properties of SmPo, the total energy is calculated. Figure 1 (a) shows the calculated total energy of this compound in B_1 and B_2 phase.

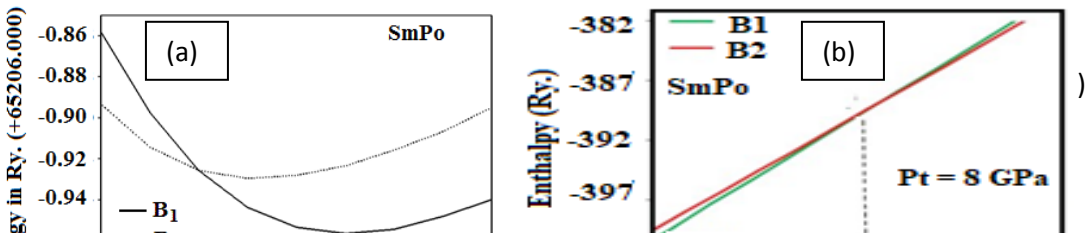

) 70

Figure 1. Variation of energy with volume for (a) SmPo and (b) Variation of enthalpy with pressure.

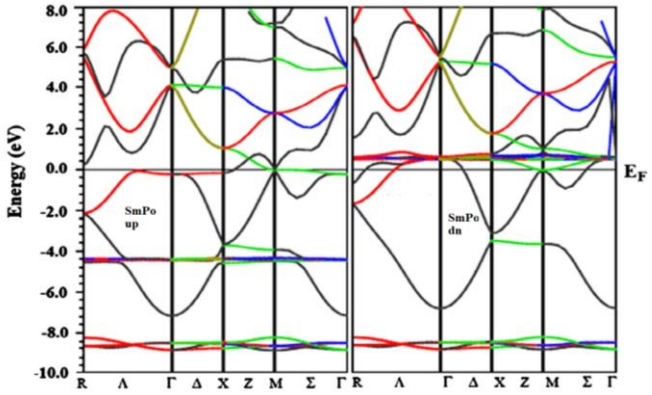

Figure 2. Band structures of SmPo in B_2-phase using LSDA approximation.

The optimized equilibrium lattice parameter, depicted in Table 1 for NaCl Structure, which appear to be in reasonable agreement with the available data [5]. To calculate the exact phase transition pressure, we have plotted the enthalpy versus pressure for SmPo and presented in figure 1 (b). This compounds has been found to undergo NaCl to CsCl structure and the calculated value of phase transition pressure is 8 GPa GPa.

The self consistent spin polarized electronic band structure calculations along high symmetry directions for SmPo using LSDA are carried out and the results presented in figure 2 where Fermi Level (E_F) is considered at zero. The overlapping of conduction and valence bands in this compound at Fermi Level (E_F) shows metallic behavior.

Table 1: Calculated equilibrium lattice parameter a_0 (Å), bulk modulus B_0 (GPa), phase transition pressure P_t (GPa) and relative change in volume at transition pressure of SmPo compound in B_1 and B_2 Phases.

Solid	Lattice Constant (Å)		Bulk Modulus B_0 (GPa)		Phase Transition Pressure (GPa)	Relative Volume Change (at Pt) %
	B_1	B_2	B_1	B_2		
SmPo						
Present	6.28	3.32	51.7	43.6	8	8.80
Other	6.72[a]	---	---	---	---	---

[a] Ref.[5]

4. Conclusions

Using first-principles calculation, we have investigated the structural ansd electronic properties of SmPo. The ground state properties such as lattice parameter, bulk modulus and its pressure derivative are calculated and compared with the available results which show good agreement. The computed band structure shows metallic nature of this compound.

Acknowledgements

The authors are thankful to UGC and Department of Higher Education, Govt. of Madhya Pradesh.

References

[1] M. De and S. K. De, J. Phys. Chem. Solids **60** (1999) 337.

[2] A. Svane, G. Santi, Z. Szotek, W. M. Temmerman, P. Strange, M. Horne, G. Vaitheeswaran, V. Kanchana, L. Petit, and H. Winter, Phys. Stat. Sol. **14** (2004) 3185.

[3] A. Jayaraman, V. Narayanamurti, E. Bucher, and R. G. Maines, Phys. Rev. Lett. **25** (1970) 1430.

[4] B. Batlogg, E. Kaldis, A. Schlegel, and P. Wachter, Phys. Rev. B **14** (1976) 5503.

[5] A. Svane, V. Kanchana, G. Vaitheeswaran, G. Santi, W. M. Temmerman, Z. Szotek, P. Strange, and L. Petit, Phys Rev. B **71** (2005) 045119.

[6] P. Blaha, K. Schwarz, G.K.H. Madsen, D. Kvasnicka, J. Luitz: WIEN2k, An

Augmented Plane Wave + Local Orbitals Program for Calculating Crystal Properties, Karlheinz Schwarz, Techn. (Univeresitat Wien, Austria, ISBN 3-9501031-1-2, 2001).

[7] P. Hohenberg, W. Kohn, Phys. Rev. 136 (1964) B864.

[8] J.P. Perdew, K. Burke, M. Ernzerhof, Phys. Rev. Lett. 77 (1996) 3865.

[9] F. Birch, Phys. Rev. 71 (1947) 809.

Paper 50

Development of Smart Energy Meter for Billing System Using ESP32

Afroj M Dange[1], Shraddha C Mahakal[2]

Assistant Professor, Department of Electronic Science[1] ,Deparment of Physics[2]

Rayat Shikshan Sanstha's, Annasaheb Awate College, Manchar, Pune, India

Abstract:

Application-based communication and information exchange through the web is one of the foremost effective and progress strategies. The Internet encourages people to stay connected both inside and outside of the organisation. Physical gadgets and objects utilized for the association through the web are called the Internet of Things (IoT). These gadgets are coordinates with remote switches that allow communication by utilizing cloud administrations to store, recover and analyze the data. Headways in different innovations have been accomplished day-by-day utilizing IoT for online examination, utilization, and Sensors control, inserted frameworks, and mechanization. A mechanized domestic through IoT innovation is called Canny family, The Exertion of collecting, power utility meter perusing. IoT presents a proficient and co-successful to exchange the data of vitality customer wirelessly as well as gives to distinguish the utilization of power the most deliberate of this extension is to degree power utilization in domestic machines and create its charge naturally utilizing IoT. The vitality network must be actualized in a disseminated topology that can powerfully retain diverse vitality sources. IoT can be utilized for different applications of the keen lattice with dispersed vitality energy plant meter, vitality era and vitality utilization shrewd meter, vitality demand-side administration, and different zone of vitality generation. Moreover, this paper concentrate on the estimation of imperativeness utilization. In this work, energy is measured in units additionally item arrangement is given to form a bill for energy utilization and usage in a computer program. An IoT-based stage is made for inaccessible checking of the metering framework in real-time. The information visualization is additionally carried out on the webpage and the information bundle misfortune is examined within the inaccessible checking of the parameter. The major purpose of this project is to use IoT to automatically measure electricity use in home appliances and generate invoices on Android phones using an IoT App.The energy grid must be built in a dispersed topology suitable for dynamically integrating various energy sources. With distributed energy plant meter, energy generation and consumption smart meters, energy demand-side management, and different sectors of energy production, IoT may be used for a range of smart grid applications.

Keywords: IoT, Smart Energy Meter, ESP32, Google Firebase

Introduction:

The energy utilization can be checked by utilizing an electric gadget called an energy meter. The expense and the ordinary use of Force utilization are educated to the client to defeat high bill utilization. The Energy meter shows the number of units devoured and moves the information to both the client, what's more, the electrical board so these aides in decreasing labor. The client can view their Force usage at any time and from any location.The IoT is utilized to Wind down on/off the family apparatuses utilizing transfer and ESP32 interfacing. The target of this framework is to

screen the measure of power devoured. The wholesaler and the buyer will be benefitted by in the long run diminishing the complete force utilization. The solution to all of these problems is to track consumer load promptly to ensure accurate billing, track peak demand, and identify thresholds. These are all the characteristics that must be taken into account when designing an efficient energy billing system. The article offers especially a smart power meter that measures the properties of embedded systems, that is, the mixture of hardware and software is used to enforce the preferred functionality. This system enables the electricity department to read the meter readings monthly without a person visiting each house. [1]This may be carried out through the usage of ESP32µc that constantly displays and information the electricity meter analyzing in its permanent (non-volatile) reminiscence location. This gadget constantly information the analyzing and the stay meter analyzing can be displayed on the website to the customer on request. This device can also be used to turn off the house's power supply while it's not in use.

Proposed Work:

When various appliances consume energy, the smart meter continuously reads the value, The smart metres can show you how much energy you've used. We can observe that the meter's LED blinks repeatedly, counting the metre reading.Based on The blinking, the units are counted. [1] In this project, we're attempting to create a system using the ESP32 µc because it has WiFi and Bluetooth modules. So, this controller can be easily access to the internet. With the help of WiFi, we managed able to connect this controller to Google Firebase. Google Firebase is a free data bus provided by Google that could be used to store data in our controller. The data contained in it can be displayed to the customer by a graphical representation of that data we have captured in App mobile with the help of the internet. IoT links anything from anywhere in the universe[2](Sulthana, Naziya; N, Rashmi; Y, Prakyathi N; S, Bhavana; Kumar, 2020)By automating remote data collection, the IoT saves consumers time and money. We developed our own id-based electricity energy meters while smart energy meters have received a lot of claims all around the world in recent years. Instead of current and voltage sensors, we used meter reading pulse data in this project. IoT cloud computing is being used to store IoT data and is used as part of communication. A cloud is a server computer providing computer resources that can be accessed by anyone at times. Cloud computing is a simple technique to transfer huge amounts of data. packages generated by the IoT through the internet.

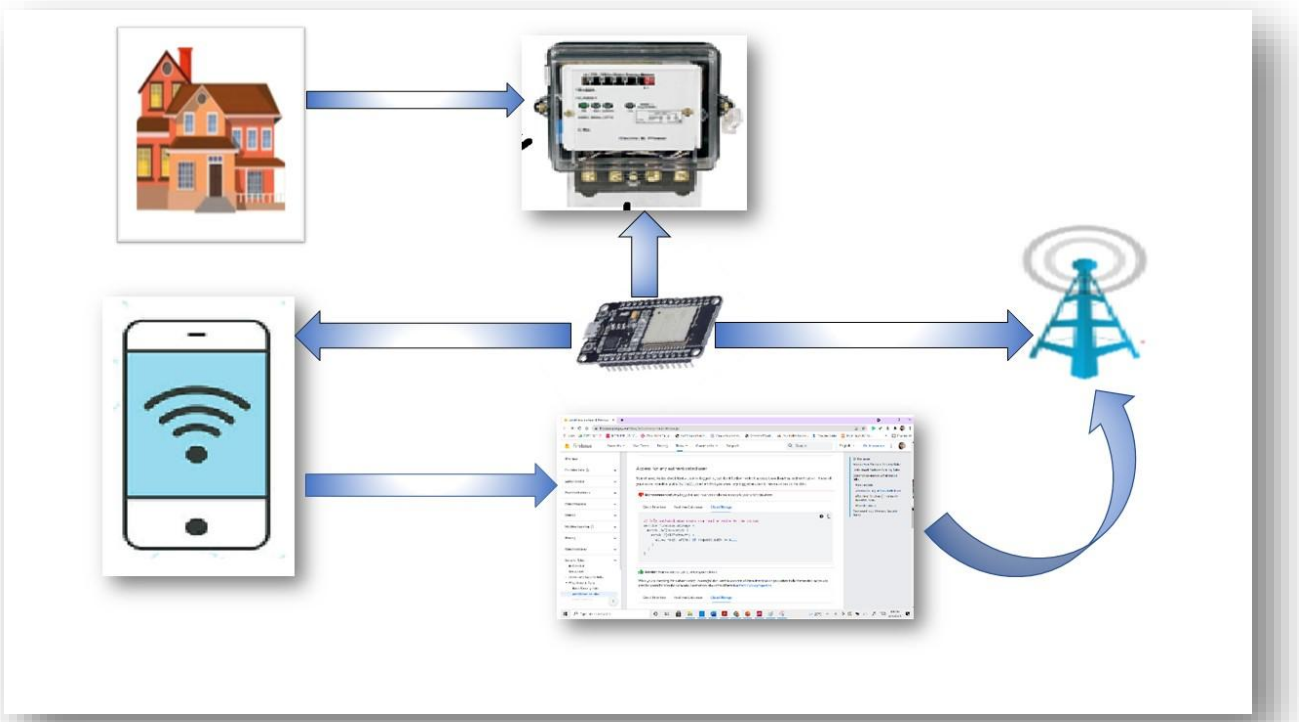

The Android App, Firebase database, and Wi-Fi Node MCU are the three major elements used in this project. The serial data 1 or 0 has been sent to the firebase database by that of the android app. The firebase database interfaces with the Wi-Fi node MCU, which also acts on the data received from the firebase database. IoT is used by Google because, the Google Cloud IoT platform helps in predicting when equipment quality enhancement and Improves actual improvement by predicting downtime, detecting, and monitoring device status, state, and position. With the help of an IoT App, you could measure and monitor power usage from anywhere. The web page makes more use of Google Firebase Analysis to perform power consumption analysis using JavaScript. That means we'll utilize Google Firebase analytics to measure our mobile app and Google Analytics to record browser significantly with an increase in HTML. Model has been proposed. The Firebase cloud can be used to connect the power board and the smart metre over internet. It eliminates human input in collecting monthly reading and saves time and costs the process of collecting electricity utility smart energy meter to use a mobile app. Any meter that consumes pulse can compute and show on an Android-based phone app.

Conclusion

The smart energy monitoring system includes ESP32c, IoT, and an energy metre. The system reads the energy meter automatically and provides home automation through an app that has been developed, along with power control. The proposed system uses less fuel and eliminates the need

for physical work.We will receive monthly energy consumption data instantly from a remote location and transfer it to the central office. This reduces the number of human works required to record energy meters, which were recorded by visiting each home individually.This concept could be expanded in the future to include prepaid power users, with the supply becoming turned on and off automatically once a customer reaches their limitation. This method can cut down on energy wastage and spread awareness among all consumers. This approach can reduce manual intervention in this situation of Covid-19 and social remoteness.

Acknowledgement: Authors are thankful to Dr. K. G. Kanade, Principal, Annasaheb Awate College, Manchar for providing support under scheme.

References

[1]D. S. A. Joshi, S. Kolvekar, Y. R. Raj, and S. S. Singh, "IoT Based Smart Energy Meter," *Bonfring Int. J. Res. Commun. Eng.*, vol. 6, no. Special Issue, pp. 89–91, 2016, doi: 10.9756/bijrce.8209.

[2]K. B. S. Sulthana, Naziya; N, Rashmi; Y, Prakyathi N; S, Bhavana; Kumar, "Smart Energy Meter and Monitoring System using IoT," *Int. J. Eng. Res. Technol.*, vol. 8, no. 14, pp. 50–53, 2020.

[3] Preethi, V., & Harish, G. (2016). Design and implementation of smart energy meter. *Proceedings of the International Conference on Inventive Computation Technologies, ICICT 2016*, *1*(August 2016). https://doi.org/10.1109/INVENTIVE.2016.7823225

[4]Sindhuja, K., Sravya, M., Rajkumar, Y., Anjali, P., Ravichander, J., & Urban, W. (2020). *Electricity Energy Meter using IoT*. 1177–1182.

[5]Okafor, K. C., Ononiwu, G. C., Precious, U., & Godis, A. C. (2017). *Development of Arduino Based IoT Metering System for On - Demand Energy Monitoring*. *7*(23), 3208–3224.

[6]Joshi, D. S. A., Kolvekar, S., Raj, Y. R., & Singh, S. S. (2016). IoT Based Smart EnergyMeter. *Bonfring International Journal of Research in Communication Engineering*, *6*(Special Issue), 89–91. https://doi.org/10.9756/bijrce.8209

[7]S. Mahmud, S. Ahmed, K. Shikder, (2019) A Smart Home Automation and Metering System Using Internet of Things (IoT), In 2019 International Conference on Robotics, Electrical and Signal Processing Techniques (ICREST), IEEE, 451-454.

[8]https://www.espressif.com/sites/default/files/documentation/esp32_datasheet_en.pdf